

02 OCT 1958

TECH LIBRARY KAFB, NM

0066907



NATIONAL ADVISORY COMMITTEE FOR AERONAUTICS

TECHNICAL NOTE 4267

PRELIMINARY SURVEY OF PROPULSION USING CHEMICAL
ENERGY STORED IN THE UPPER ATMOSPHERE

By Lionel V. Baldwin and Perry L. Blackshear

Lewis Flight Propulsion Laboratory
Cleveland, Ohio



Washington

May, 1958

AFMDC
TECHNICAL LIBRARY
AFL 2811

NACA TN 4267

80901



0066907

NATIONAL ADVISORY COMMITTEE FOR AERONAUTICS

TECHNICAL NOTE 4267

PRELIMINARY SURVEY OF PROPULSION USING CHEMICAL
ENERGY STORED IN THE UPPER ATMOSPHERE

By Lionel V. Baldwin and Perry L. Blackshear

SUMMARY

This report presents a preliminary study of a ramjet that would use the chemical energy of dissociated molecules in the ionosphere for propulsion. A review of the physical properties and chemical composition of the upper atmosphere shows that the available energy is not sufficient for flight requiring aerodynamic lift. Above 300,000 feet, dissociation energy might be useful for satellite-sustaining. Comparison of maximum thrust and external drag for an orbiting ramjet from 300,000 to 700,000 feet shows that a positive net-thrust margin might be obtained over the entire region for some of the engine sizes considered. However, the region between 325,000 and 400,000 feet is the most favorable, because high gas densities produce high recombination rates.

Two thermodynamic engine cycles are considered for a ramjet orbiting at 328,080 feet: (1) all-supersonic flow with frozen composition in the diffuser and chemical equilibrium in the nozzle; (2) normal-shock inlet with equilibrium expansion. Only the all-supersonic cycle shows promise for sustaining a satellite. Calculations of the rate of recombination are only approximate because of uncertainties in the data on the chemical reaction rates. These approximate calculations indicate that, although equilibrium expansion cannot be obtained, up to 50-percent recombination may be possible for a nozzle 100 feet long. This would give thrust in excess of the drag.

Aerodynamic-heating problems of the orbiting ramjet are considered. External surfaces are sufficiently cooled by radiation. The internal throat area, which presents the most difficult cooling problem, requires cooling rates that are met by current technology; but, in order to minimize heat loss due to internal cooling, the inlet radius of the engine will probably have to be greater than 20 feet for an engine 100 feet long.

The recombination ramjet appears to be a marginal device even in the optimistic view. Before definite conclusions can be drawn, the

4780

CY-1

atmospheric composition near 300,000 feet and the recombination-rate coefficient for atomic oxygen must be accurately known. If favorable composition and rate coefficients are measured in future research, then the "fuelless" recombination ramjet can probably be developed, but only for use where most of the lift comes from the orbiting velocity.

INTRODUCTION

About 75 years ago, W. N. Hartley observed the abrupt termination of the ultraviolet end of the spectrum of all heavenly bodies and postulated the existence of ozone in the Earth's atmosphere to account for this absorption. In 1930, Sydney Chapman showed theoretically that the absorption of solar ultraviolet light should cause diatomic oxygen to dissociate at altitudes above 100 kilometers. The theory was clear-cut and was universally accepted, although the atomic oxygen in the ionosphere had not been experimentally measured. More recent theories have postulated that nitrogen is also dissociated in the upper regions of the ionosphere. Balloon experiments and, in the last ten years, high-altitude rockets have proved these speculations to be correct.

A small fraction of the solar energy absorbed by the Earth is locked in reactive chemical species such as ozone, dissociated molecules, and gaseous ions in the upper atmosphere. This energy may be available for flight propulsion in the upper atmosphere. For example, in 1950, Proell (ref. 1) proposed the use of "fuelless box-ramjets" using the energy of atomic oxygen at about 100 kilometers to move and direct space stations, alter orbits, and overcome frictional losses. The "fuelless" feature of an engine that converts the chemical energy of reactive air particles into thrust is very attractive for these applications. Furthermore, the simplicity of the ramjet is desirable where long service times are required.

The availability of atmospheric energy for propulsion is investigated in detail in this report in the light of atmospheric data obtained by rockets in the last five years. To facilitate the ramjet cycle calculations, the reaction enthalpy for the conversion of photochemically dissociated air to stable molecules in equilibrium is summarized as an available energy density (Btu/cu ft of air) for altitudes from 50,000 to 1,000,000 feet. An analysis comparing the available energy with the energy required for flight shows that sufficient thrust can be provided only by an orbiting engine.

Next, the orbiting ionosphere ramjet is considered in detail. The external drag for various nacelle geometries is compared with the maximum available thrust from 325,000 to 700,000 feet. One of the more promising flight altitudes and configurations is chosen for a thermodynamic cycle calculation. Finally, the problems of recombination chemical kinetics

4780

and internal and external heat transfer are examined for this ramjet orbiting at 328,080 feet. The calculation of heat transfer and friction drag is discussed in appendix D by James F. Schmidt.

Unfortunately, existing data are not complete enough to evaluate definitely the recombination ramjet. The purpose of this report is to present a preliminary study and to point out the research data that are necessary. By making plausible assumptions where data are lacking, it is possible to propose the major design requirements and to indicate the probable magnitude of the problems likely to be encountered.

MODELS OF UPPER ATMOSPHERE

Physical Properties

The pressure, density, temperature, and composition of the atmosphere extrapolated up to an altitude of 1,600,000 feet are summarized in engineering units in tables I to III. Three data summaries of upper-atmospheric rocket research (refs. 2, 3, and 4) have been selected to serve as "standard atmospheres" for this discussion. The combined results of all rocket flights from 1946 to January 1952, presented by the Rocket Panel (ref. 2), are summarized in table I. Another summary (ref. 3) was prepared by Dr. E. O. Hulburt, Director of Research at the Naval Research Laboratory. Hulburt presented smoothed, average values obtained by all flights up to July 1954, and he extrapolated the data from 725,000 to 1,600,000 feet. This working model of the atmosphere is presented in table II. A more recent standard atmosphere (1956) has been proposed as the Air Force ARDC Model Atmosphere (ref. 4). Table III is an abridged form of this model.

Symbols are defined in appendix A, and the reliability of the tabulated physical properties of the atmospheric models is discussed briefly in appendix B.

Chemical Composition

The chemical compositions in tables I to III are less certain than the physical properties, because composition data above 250,000 feet are very scant. In fact, the compositions in table I are hypothetical; the Rocket Panel assumed these values only to calculate an average molecular weight, which in turn could be used to calculate temperature from measured pressure and density. As discussed in appendix B, the Hulburt-NRL model compositions from 357,000 to 420,000 feet (table II) are based on data from three Aerobee rocket flights in 1953. Above 426,000 feet, the compositions are based on assumed atmospheric conditions. The ARDC compositions of table III were prepared from smoothed individual particle

concentrations read from a graph published in reference 5. Therefore, table III compositions are approximate, but they probably represent the ARDC adopted values within 3 percent for any component. Appendix B includes a discussion of the compositions of the three model atmospheres.

The chemical energy associated with the nonequilibrium composition of "air" at these high altitudes has been estimated from the tabulated composition data of tables I and II (fig. 1). The available chemical energy is taken to be the reaction enthalpy for the conversion of the photochemically dissociated air to stable molecules in chemical equilibrium. Chemical propulsion schemes based on the presence of ozone, atomic oxygen, and atomic nitrogen can be evaluated readily from figure 1, which shows "available chemical-energy density" (Btu/cu ft of air) from 50,000 to 1,000,000 feet. Table III energy density, though not shown, would be between the Rocket Panel and Hulburt-NRL curves in the region from about 300,000 to 600,000 feet.

The calculation procedure used to obtain figure 1 from tables I and II, together with some additional composition data on ozone (table IV), is included in appendix B. Therefore, only a qualitative description of figure 1 will be given here. The solid curve between 50,000 and 260,000 feet represents the chemical energy of ozone, which is not shown in either table I or II because it is present in only minute concentrations. The vertical line at 270,000 feet emphasizes the uncertainty of the Rocket Panel's assumed composition at this altitude; actually, the abrupt rise in atomic oxygen concentration listed in table I would lead to a nearly vertical slope. The solid curve from 270,000 to 394,000 feet is the energy density associated with atomic oxygen; above 394,000 feet, atomic nitrogen begins to contribute with increasing importance.

For the energy-density curve from the Hulburt-NRL model of table II, the atomic oxygen begins to contribute to the energy density at about 150,000 feet. The dashed curve from 150,000 to 325,000 feet reflects a rapid buildup of atomic oxygen concentration which, though below 2 percent of the total air, is still significant in terms of energy because of the relatively high total air density. Because the atomic oxygen concentrations are small in this transition region from 150,000 to 325,000 feet, the percentages are not listed in table II but are included in table IV instead. The peak in the dashed curve (fig. 1) at about 320,000 feet is caused by the leveling off of the initially steep increase in percentage of atomic oxygen in the transition region to the values shown in table II above 328,000 feet. The slope of this curve following the peak reflects the exponential decrease in total air density. Atomic nitrogen starts to contribute to the energy at about 460,000 feet, causing the change in slope shown in figure 1.

THE IONOSPHERE RAMJET

Assuming that the atmospheric energy described in the previous section is available for propulsion, it is important next to determine the flight speeds and altitudes at which this energy would be sufficient. Such an orienting analysis is presented in appendix C, which formalizes the relations concerning required energy, lift-drag ratios, engine efficiency, friction drag, altitude, and flight speed. This analysis shows that for a supersonic ramjet the available energy would not be useful for sustaining flight requiring aerodynamic lift. However, for an orbiting ramjet the available energy may be sufficient to overcome friction drag above about 300,000 feet.

Therefore, an orbiting ionosphere ramjet is considered in this section. Appearance, operation, and design problems are discussed. No attempt is made to consider all possible engine designs. Rather, one plausible ramjet is studied in detail to test the feasibility of using atmospheric energy. The external friction drag for various truncated-cone nacelle geometries and orbit altitudes is presented first. Then, for a promising configuration and altitude, a thermodynamic cycle is followed through to determine some factors influencing engine efficiency. Since the chemical kinetics for the recombination of dissociated air will govern the actual engine cycle, the assumptions used in the thermodynamic analysis are examined with respect to the kinetics. Finally, since aerodynamic heating can destroy an object orbiting in the atmosphere, the internal and external heat-transfer problems are considered.

Thrust-Drag Comparison at Various Altitudes

The thrust F of a recombination ramjet is easily related to the energy density e of the air at the orbit altitude. The thrust per unit inlet area A_1 is

$$\frac{F}{A_1} = \eta e J \quad (1)$$

The thrust is a function of engine efficiency η and altitude, since e depends on altitude. If the engine efficiency is assumed to be 100 percent, then it is convenient to define a thrust parameter that is a function only of orbit altitude:

$$\frac{F}{A_1 \rho_1} = \frac{e J}{\rho_1} \quad (2)$$

The thrust parameter has been evaluated for altitudes from 300,000 to 700,000 feet using the two model atmospheres of figure 1. The two

curves of figure 2 represent the probable upper and lower limits on the energy available for propulsion for a recombination ramjet at orbital velocity.

A similar term can be defined for external drag, but the nacelle geometry must also be specified. Figure 3 shows the simple truncated-cone nacelle geometries considered in this preliminary study. Nacelles having these shapes can be distinguished for the following discussion by giving the ratio of length to capture radius \mathcal{L}/R_1 , the cone half-angle θ , and the over-all length \mathcal{L} . A variety of combinations of the three variables was chosen, and the external drags for each nacelle were calculated over an altitude range. In the friction-drag calculations outlined in appendix D, a procedure described by Eckert (refs. 6 and 7) was used. The external drag is divided by the inlet area and ambient density for direct comparison with the maximum thrust.

The energy available is compared with the energy required to overcome drag for altitudes from 300,000 to 700,000 feet and for \mathcal{L} of 100 and 1000 feet in figures 4(a) and (b), respectively. Figure 4(b) is intended only to show the effect of engine size on external drag and maximum thrust over a wide range. Both plots give the drag parameter for \mathcal{L}/R_1 of 2.5, 5, 10, and 30, and for θ of 2° , 0° , -4.3° , and -8.6° .

The requirement for sustained satellite flight is

$$\frac{F}{A_1 \rho_1} \geq \frac{D}{A_1 \rho_1} \quad (3)$$

Figure 4 indicates that, even with an engine efficiency of 100 percent, the smallest engine size shown ($\mathcal{L} = 100$ feet) would not sustain satellite flight unless very small \mathcal{L}/R_1 and negative θ could be used. As might be expected, larger inlets give increasingly favorable thrust margins with this idealized comparison.

The difference between the thrust and drag parameters in figure 4 is proportional to the maximum net thrust. Between altitudes of 320,000 and 400,000 feet, four of the design configurations show positive net-thrust capabilities. It will be shown later that the chemical recombination reaction is strongly influenced by air density, being more favorable as density increases. Furthermore, the drags in figure 4 are probably too low above 450,000 feet, because the flow would be approaching free-molecule flow (see appendix C). Therefore, for the following cycle analysis, 328,080 feet was chosen as a favorable altitude, although this precise choice was arbitrary.

Thermodynamic Cycle for Recombination Ramjet

The engine efficiency of a recombination ramjet will certainly be less than 100 percent, and the nacelle geometry can be expected to affect efficiency as the ratio of inlet to exhaust area (and therefore the degree of expansion) is varied. These performance variables and others are discussed in the following paragraphs.

4780 The problem is to get the energetic ambient air on board, to recombine the atomic oxygen, to exhaust the hot diatomic air, and thus to obtain thrust. A circular orbit of 328,080 feet and the atmosphere of the Rocket Panel (table I) are the assumed flight conditions. Two different cycles are analyzed. However, it should not be inferred that these include all possible cases.

All-supersonic cycle. - The first cycle is an all-supersonic cycle; that is, the flow throughout the engine is above sonic velocity. The cycle can be divided into three stages, as follows: (1) frozen-composition compression, (2) conversion of compressed air to chemical equilibrium, and (3) chemical-equilibrium exhaust expansion to ambient pressure. There is an apparent paradox in these assumptions, because the first requires the recombination rate to be zero, while the third assumes that the rate is fast compared with flow residence times. For the moment, assume that each limiting condition could be approached by making the diffuser residence time short compared with the exhaust-nozzle flow time. Later, a kinetic analysis will estimate the accuracy of these limiting assumptions.

Unfortunately, the published thermodynamic properties for air do not extend over the entire low-pressure region of this cycle (e.g., ref. 8). However, a report on the thermodynamic properties of the three-component hydrogen-oxygen-nitrogen system has recently been published (ref. 9). This system is available at the NACA Lewis laboratory in a digital-computer program designed to study rocket nozzle performance. The simple expedient of driving the hydrogen content to negligible proportions (10^{-10} percent or less) converted the hydrogen-oxygen-nitrogen system of reference 9 to an argon-free air system that included the entire pressure range of interest here. All thermodynamic properties used in this section were obtained from this program and reference 9, using "air" with 1 mole of oxygen (32.000) for every 3.773 moles of nitrogen (28.016).

Figure 5(a) shows the thermodynamic cycle on a plot of static temperature against static pressure. Figure 5(b) gives the corresponding air enthalpy as a function of static pressure. The three stages of this cycle are discussed briefly in the following paragraphs.

For the 328,080-foot orbit, the frozen composition is 19 percent O (by volume), 9.5 percent O₂, and 71.5 percent N₂. The enthalpy H_T at any temperature station in the compression is given by

$$H_T = \left[0.19(\mathcal{H}_O)_T + 0.095(\mathcal{H}_{O_2})_T + 0.715(\mathcal{H}_{N_2})_T \right] \frac{1}{26.11} \quad (4)$$

The air enthalpy of figure 5(b) was calculated from equation (4) and the molar enthalpies \mathcal{H}_i tabulated in reference 9 for all T. The relation between temperature and pressure for the frozen compression was assumed to be that for isentropic flow:

$$\frac{P_{II}}{P_I} = \left(\frac{T_{II}}{T_I} \right)^{\frac{\gamma}{\gamma-1}} \quad (5)$$

Since the exponent $\gamma/\gamma-1$ is a function of temperature, a small temperature difference ($T_{II} - T_I = 180^\circ \text{R}$) was used, and the pressure ratio was calculated for these temperature increments. Reference 9 data on C_p/\mathcal{R} for the individual chemical components were averaged on a molar basis (as in eq. (4)) for use as $\gamma/\gamma-1$. Therefore, the compression in both enthalpy-pressure and temperature-pressure relations includes an allowance for adjustment in specific heats.

The problem of where to terminate the compression is unique to the recombination-ramjet cycle. The procedure used to calculate the compression-termination station, where the conversion of frozen to equilibrium is assumed to occur, is illustrated by figure 5(c). This figure is simply an enlarged temperature-pressure diagram in the region near station 2 of figure 5(a).

If the frozen compression is assumed to persist until very high static temperature is attained, then the conversion of the ambient composition air to equilibrium will lead to more dissociation and a temperature drop. To illustrate, consider station b (fig. 5(c)), which is an arbitrary station in the frozen compression. The constant-pressure adiabatic conversion from frozen to equilibrium causes a temperature drop to T_b . On the other hand, let the compression be terminated at a low pressure (station a). Then recombination occurs when the gas is converted at constant pressure to equilibrium, and a temperature rise to T_a is noted. The compression-termination station 2 in figures 5(a) and (b) is the adiabatic, isobaric, isothermal conversion of the frozen inlet air to equilibrium.

It is not apparent from the preceding discussion that station 2 is the most advantageous conversion point, and indeed it might not be.

However, of the three points discussed, the isothermal conversion was observed to give higher engine efficiency with full expansion than either station a or station b. This efficiency difference was small, being less than 1 percent for all three cases. Therefore, the choice of any other conversion station in the region shown in figure 5(c) rather than station 2 would have had negligible effect on the results of the cycle analysis.

The final stage of the cycle is an isentropic expansion in chemical equilibrium from station 2 to station 3. In figure 5(a), note the unusual temperature-pressure dependence from station 2 down to about 10^{-1} pound per square foot; in this region the recombination of atomic oxygen is occurring. The release of the chemical energy is also shown clearly on the enthalpy-pressure plot (fig. 5(b)).

The chemical composition during the equilibrium expansion from stations 2 to 3 is given in figure 6. At station 2, the difference between the inlet frozen composition and the composition of the equilibrium mixture is due solely to 2.23 percent NO. The equilibrium compositions of figure 6 are used in the chemical kinetics analysis of the next section.

The ideal engine efficiency and the net thrust were calculated from the cycle summarized in figures 5 and 6. The flow conditions at the throat (station 2) are as follows:

$$U_2 = \sqrt{U_1^2 - (H_2 - H_1)2g_c J} \quad (6)$$

where

$$U_1 = 26,050 \text{ ft/sec (orbital velocity)}$$

$$\left. \begin{aligned} H_1 &= 984.8 \text{ Btu/lb(M)} \\ H_2 &= 2309.4 \text{ Btu/lb(M)} \end{aligned} \right\} \text{ fig. 5(b)}$$

$$U_2 = 24,743 \text{ ft/sec}$$

$$M_2 = \frac{U_2}{\sqrt{\gamma \mathcal{R} g_c T_2}} = 7.5 \quad (7)$$

and the ratio of inlet to throat area is calculated from continuity:

$$\frac{A_1}{A_2} = \frac{U_2}{U_1} \frac{T_1}{T_2} \frac{P_2}{P_1} \frac{\bar{M}_1}{\bar{M}_2} \quad (8)$$

$$= 740.6$$

The average molecular weights \bar{M} at stations 1 and 2 were calculated from compositions given in table I and figure 6.

In a similar manner, the ratios of throat to exit velocity and throat to exit area were evaluated at various stations throughout the equilibrium expansion. Then, the thrust per unit inlet area was determined from

$$\frac{F}{A_1} = \frac{\rho_1 U_1}{g_c} (U_3 - U_1) + P_3 \left(\frac{A_3}{A_1} \right) - P_1 \quad (9)$$

That is, the thrust depends on the inlet area and the ratio of inlet to exit area. If truncated-cone nacelles are used, then the drag also depends on the ratio of inlet to exit area. This suggests that an optimum area ratio exists, as will be discussed shortly.

Closely related to the thrust is the engine efficiency:

$$\eta = \frac{F}{A_1 e J} \quad (10)$$

The Rocket Panel energy density e from figure 1 at 328,080 feet was substituted into equation (10) together with the results from equation (9). The resulting engine efficiency is given in figure 7 as a function of A_1/A_3 .

If the thermodynamic cycle assumptions of equilibrium expansion and reversible adiabatic flow are good approximations, then an optimum configuration for maximum net thrust can be found. Figure 8 gives the thrust and drag as a function of the ratio of inlet to exit area for a 100-foot engine having an inlet radius of 20 feet. The drag is much more sensitive to this area ratio than the ideal thrust, and it is clear that the difference between thrust and drag will pass through a maximum. Figure 9 shows the net thrust for engines 100 feet long with various inlet radii as a function of ratio of inlet to exit area. The large effect of inlet radius could be expected, because the thrust is directly proportional to the inlet area, or $(R_1)^2$, while the drag is proportional to the nacelle surface area, or approximately R_1 . The optimum net thrust peaks more sharply for large inlets, but in all cases shown the peak occurs at area ratios between 2 and 6; the corresponding cone half-angles are negative, about -4° to -6° .

Normal-shock-inlet cycle. - The cycle discussed has assumed that the flow in the orbiting ramjet is supersonic throughout. Many alternative cycles involving shock inlets are possible, of course, but only the extreme case of a normal-shock-inlet cycle has been examined for this preliminary study. Appendix E gives an analysis of a recombination

ramjet with a normal-shock inlet under the identical flight conditions of the supersonic analysis. This analysis shows that the extremely high static temperatures after shock result in more dissociation than can be regained in a full equilibrium expansion. A ramjet with a normal-shock inlet in a 328,080-foot orbit failed to produce useful thrust by at least an order of magnitude.

Chemical Kinetics of Recombination

The recombination ramjet could supply sufficient thrust to sustain itself indefinitely in circular ionosphere orbits under ideal circumstances: reversible, adiabatic flow and chemical-equilibrium nozzle expansion. In this section the assumptions of frozen-composition compression and chemical-equilibrium nozzle flow are examined; the next section is concerned with the heat-transfer problem.

If the chemical rate processes were understood completely and all kinetic data were available, the problem of adiabatic nozzle expansion with chemical reactions would be solvable, at least in principle. However, even for the simple case of recombining atomic oxygen in the absence of foreign fuels, plausible assumptions must replace data that are lacking today. The recombination kinetics are analyzed here for two limiting conditions to place upper and lower limits on the probable degree of recombination. The limiting cases considered are:

(1) Near-equilibrium flow: This condition would occur if the recombination of the atomic oxygen were sufficiently rapid to keep pace with the shift of equilibrium compositions resulting from the drop in static temperature and pressure in the nozzle flow.

(2) Near-frozen-composition flow: In this case the recombination kinetics are so slow that negligible recombination occurs.

The details of the kinetic analysis are deferred to appendix F, where the general method described in reference 10 is applied to recombination of atomic oxygen in the exhaust nozzle. However, a qualitative understanding of the analysis is sufficient to make the results meaningful. In an actual nozzle, the flow may either be in chemical equilibrium, have frozen composition, or vary anywhere between these limiting cases depending on the reaction rate. For example, consider a hypothetical nozzle with a very large pressure ratio. The nozzle flow could follow chemical equilibrium initially. As the recombination proceeds, the concentrations of atomic oxygen reactants would drop to such low values that the reaction rates could no longer keep pace with the minimum rate required for near-equilibrium flow. The reaction would proceed in the nozzle with rapidly decreasing rate as the atomic oxygen was converted to molecular oxygen; but eventually the rate would become

so slow that, for all practical purposes, no more recombination would occur. At the latter condition, the flow is at the other limit, near-frozen-composition flow. The analysis of the nozzle flow given in appendix F makes possible the numerical evaluation of the minimum concentration of atomic oxygen that would exist in a given nozzle when the flow deviates from equilibrium because of insufficient reaction rate. The analysis also places an upper limit on the atomic oxygen concentration corresponding to a reaction rate which, if exceeded, would cause the flow to deviate from near-frozen composition.

The numerical example summarized in table V is for the nozzle expansion discussed in the supersonic cycle. The first column lists recombination-rate coefficients k_f from 10^{11} to 10^{16} (g-mole/liter)⁻² sec⁻¹; cgs units are used here for convenience, because these are the usual units used by physical chemists reporting kinetic data. Only one value of k_f would be listed if rate data were available; but, as will be discussed shortly, there is enough uncertainty concerning k_f to warrant the wide range of magnitudes in the table.

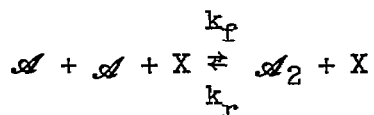
The second column in table V gives the minimum concentration of atomic oxygen (\mathcal{C}_O , g-mole O/liter) required for near-equilibrium flow with the corresponding rate coefficient. Atomic oxygen concentrations smaller than those shown would cause the flow to deviate toward frozen flow. However, atomic oxygen concentration depends not only on the mass fraction of atomic oxygen but also on the air density, and both vary in the nozzle flow. That is, the minimum concentration necessary for near-equilibrium flow is meaningless as a guide to recombination, unless it is related to the temperature, pressure, and mean molecular weight of the expanding air. If it is recalled that the air is assumed to follow chemical equilibrium until the minimum concentration for near-equilibrium is reached, then it follows that the equilibrium concentrations in figure 6 together with the temperature-pressure relation in figure 5(a) give the required relation between temperature, pressure, mean molecular weight, and the mass fraction of atomic oxygen. For equilibrium flow, appendix F shows that the mass percentage of atomic oxygen recombination can be calculated as a function of the atomic oxygen concentration in the nozzle flow. Figure 10 is a plot of this relation. The minimum \mathcal{C}_O values in table V are related by figure 10 to the mass percentage of the atomic oxygen that has recombined to molecular oxygen; this number is significant, since it sets a lower limit on the amount of recombination attained if the rate coefficient is k_f .

The last two columns of table V give similar results for near-frozen flow in the nozzle. If \mathcal{C}_O is smaller than the listed values at the given k_f , then negligible recombination will occur. The relation

between \mathcal{C}_0 and mass percentage recombined cannot be determined rigorously for the near-frozen process by this simple analysis, because the necessary flow relations are unknown once the flow varies from equilibrium. However, by assuming the equilibrium flow relation between \mathcal{C}_0 and mass percentage recombined (fig. 10), it is possible to set an upper limit on the degree of recombination. Regardless of what the actual reaction rate is in the intermediate flow between equilibrium and frozen, it will certainly be slower than in equilibrium flow. Therefore, the corresponding mass percentage recombined given in the table was taken from figure 10, and it is the maximum degree of completion possible in the nozzle for a particular value of k_f .

A recombination-rate coefficient of 10^{11} (g-mole/liter) $^{-2}$ sec $^{-1}$ is frequently employed by physical chemists for reactions of this type, because, although no experimental data for atomic oxygen are available, values of k_f of 10^{10} have been observed for iodine, bromine, deuterium, and hydrogen atomic recombinations (ref. 11). Furthermore, the reaction rates were found to be almost temperature-independent, with activation energies near zero. This is the only justification for referring to single-valued k_f in a nozzle where the temperature varies over a 4000 $^{\circ}$ F range. If 10^{11} were correct, then the flow would never approach chemical equilibrium, and 8-percent recombination would occur at most. Under these circumstances, the ionosphere ramjet would not be feasible.

Fortunately, there is reason to believe that the rate constant for recombination of atomic oxygen may be much larger than 10^{11} . Feldman (ref. 12) has recently reported an interesting high-temperature shock-tube study of the kinetics of "air." Air was dissociated at the high temperatures following the passage of the shock through the tube, and a preliminary experiment established that the dissociated air was in chemical equilibrium. The hot equilibrium air was then passed over a reversed wedge in a Prandtl-Meyer expansion. By observing Mach angles in the expansion, Feldman was able to conclude that the air had maintained chemical equilibrium throughout the rapid drop in static temperature and pressure. By using an analysis similar to that given in appendix F, he calculated lower-limit recombination-rate coefficients k_f from 4500 $^{\circ}$ to 7900 $^{\circ}$ K and from 0.005 to 1 atmosphere for the following reaction:



where \mathcal{A}_2 represents a molecule of "air" and \mathcal{A} an atom of "air" having half the molecular weight of the molecule. Lower-limit coefficients k_f as high as 10^{13} (g-mole/liter) $^{-2}$ sec $^{-1}$ were reported.

If 10^{13} is the correct k_p , then table V indicates that, although near-equilibrium flow would not be attained anywhere in the nozzle, over 50-percent recombination is possible in a nozzle 100 feet long. The results of the AVCO shock-tube research can probably be applied to the recombination of oxygen, because atomic oxygen is the predominant dissociation species of "air" in the temperature-pressure region where 10^{13} was deduced.

The effect of changing the length of the adiabatic nozzle can also be obtained from table V. The values shown are for a 100-foot nozzle, but it is reasonable to expect that going to longer nozzles will give more time for recombination. Equations (F16) and (F21) of appendix F give this quantitative statement. For example, if the nozzle were 1000 feet long, then the effect would be to divide each k_p in table V by 10. Thus, for $k_p = 10^{13}$, up to 78-percent completion might be expected, but equilibrium flow would not be approached anywhere in the nozzle.

The preceding discussion of table V assumes that the inlet-diffuser flow will have frozen composition. If recombination-rate coefficients of 10^{13} or less are correct, then the assumption of frozen inlet flow is probably much better than the assumption of equilibrium nozzle flow. This is especially true where the inlet diffuser length is about 10 feet compared with at least 100 feet for the exhaust nozzle. The major problem will be obtaining sufficient recombination. Any recombination occurring in a short diffuser will simply reduce both the design temperature and the pressure at station 2. That is, the limiting cycle of figure 5(a) probably envelops the actual cycle, which would have (1) a slightly steeper temperature-pressure dependence toward the end of the compression, (2) a lower temperature-pressure design station for the start of the nozzle expansion, and (3) a steeper temperature-pressure curve in expansion with less pronouncedly flat recombination region. Naturally, the enthalpy difference between stations 1 and 3 would be less than the limiting cycle, because, unlike that in figure 5, the exhaust gas would probably have some dissociation energy. The actual thrust would be less than that calculated in this cycle analysis.

A kinetic solution to give values for the actual cycle outlined in general will not be attempted here. The uncertainties in both atmospheric composition and reaction-rate coefficient are much too large to justify laborious "exact" numerical designs. However, if about 50-percent conversion could be obtained in an engine about 100 feet long, then by making the capture radius R_1 sufficiently large, the recombination ramjet principle would be worthy of further study.

The chemical kinetics of recombination are very sensitive to orbit altitude, since the reaction rate is roughly proportional to the cube of the ambient density. The results in table V are applicable to an

altitude of 328,080 feet in the atmosphere of table I, which is the lowest region of appreciable photochemical dissociation in this model. Lower orbits, though desirable kinetically, appear to be impossible.

Heat-Transfer and Cooling Problems of Orbiting Ramjet

External. - The external equilibrium wall temperature for the reverse truncated-cone nacelle is radiation-controlled. Figure 11 gives the results of a calculation of the wall temperature at the 100-foot point on a -8.6° nacelle over an altitude range from 328,000 to 750,000 feet. The calculation assumed that the surface of the nacelle was normal to the sun's rays and that it radiated energy as a black body to space (see appendix D). Within the accuracy of the calculation, the convective heat transfer did not contribute at $\mathcal{L} = 100$ feet; but, for cone half-angles more positive than -8.6° , a small variation in the wall temperature was noted over this altitude range. The variation of wall temperature over the length of the nacelle is given by figure 12. An orbit altitude of 328,080 feet was chosen for this example, and the wall temperatures for cone half-angles of -4.3° and -8.6° are typical of the effect of convective heat transfer on the surface linear dimension. The important conclusion to be drawn from figures 11 and 12 is that, because of radiation cooling, external heating will not be a problem.

Internal. - The internal surface, having no radiant cooling outlet, presents the major cooling problem of the orbiting ramjet. The throat of the engine (station 2) is most difficult to cool, because the maximum heat-transfer rates occur there. To estimate the magnitude of the problem, consider a ramjet with R_1 of 20 feet orbiting at an altitude of 328,080 feet. The ratio of inlet to throat area A_1/A_2 from the cycle calculations is 740.6.

The heat-transfer coefficient is calculated from station 2 conditions and the Dittus-Boelter equation, which is commonly used in rocket throat cooling problems (ref. 13). As shown in appendix D, the maximum heat-transfer rate for the throat of this ramjet is

$$\frac{q}{A_s} = 10.82 \frac{\text{Btu}}{(\text{sec})(\text{sq ft})}$$

Current rocket practice for throat cooling can handle heating rates as great as 100 times 10.82. Therefore, the hot-spot cooling for the orbiting recombination ramjet could be solved with present technology, the problem being less difficult than that encountered in rocket design.

Of course, the entire internal surface of the engine will require cooling. The cooling system might use the outer nacelle as a radiator

and use a coolant in a continuous cycle. The heat transferred by the radiator could make the ramjet inoperative if this heat were a large fraction of recombination energy, because this radiated energy is not available for propulsion. The fraction of the heat lost in cooling will depend on the geometry of the engine and the orbit altitude, but it is interesting to make a crude analysis at 328,080 feet to complete this preliminary survey.

The heat-transfer rate at any section of the internal surface is

$$\frac{dq}{dA_B} = h_C(T_{aw} - T_w) \quad (11)$$

The adiabatic wall temperature will vary only slightly in the engine at hypersonic speeds; therefore, if it is assumed that the wall temperature is maintained constant throughout, $T_{aw} - T_w$ does not vary in the engine. By substituting the Dittus-Boelter equation for the heat-transfer coefficient (appendix D, eq. (D19)), equation (11) becomes

$$\frac{dq}{dA_B} = 0.023 \frac{x_f}{d} \left(\frac{\rho U d}{\mu_f} \right)^{0.8} \left(\frac{C_p \mu}{\kappa} \right)_f^{0.33} (T_{aw} - T_w) \quad (12)$$

The velocity is nearly constant in hypersonic flow; therefore, from continuity the following approximations can be made:

$$U \approx \bar{U} = 26,000 \text{ ft/sec} \quad (13)$$

$$\rho d^2 \approx \rho_1 d_1^2 \quad (14)$$

Equation (12) can be written in terms of equations (13) and (14) for the total cooling required:

$$q_{\text{cooling}} = \left[0.023 \pi x_f \text{Pr}_f^{0.33} \left(\frac{\bar{U}}{\mu_f} \right)^{0.8} (T_{aw} - T_w) \rho_1^{0.8} d_1^{1.6} \right] \int_0^L \frac{dx}{d^{0.8}} \quad (15)$$

The numerical value of equation (15) depends strongly on the inlet diameter d_1 and to a lesser extent on the internal design (i.e., $d = f(x)$). The greatest value of q_{cooling} for any inlet diameter would occur in an engine for which the length average internal diameter approaches the throat diameter d_2 . Since d_2 is related to d_1 by continuity, this maximum cooling load for the ramjet discussed for the supersonic cycle ($A_1/A_2 = 740$) is

$$q_{\text{cooling}} = \pi 0.682 d_1^{0.8} \mathcal{L} \quad (16)$$

The total heat added to the system per second is

$$E_{\text{added}} = U_1 A_1 e \quad (17)$$

At a 328,080-foot orbit altitude, with e from figure 1, this is

$$E_{\text{added}} = \pi d_1^2 \quad (18)$$

Therefore, the desired crude formula for the maximum fraction of heat lost by cooling is obtained by combining equations (16) and (17):

$$\text{Maximum fraction heat lost} = \frac{0.30 \mathcal{L}}{R_1^{1.2}} \quad (19)$$

where R_1 and \mathcal{L} are in feet.

Equation (19) is not a useful rule of thumb for estimating the departure of the engine from adiabatic, because the assumption of equation (16) is probably too severe on the internal design. For example, if the engine is 100 feet long and the inlet radius is 20 feet, about 80 percent of the recombination energy would be unavailable for propulsion because of internal cooling.

An optimistic value of the cooling load can also be obtained from equation (15), which sets a lower limit on the cooling required. By assuming that the length average internal diameter is equal to the inlet diameter (rather than to the throat diameter), the following equations are obtained:

$$q_{\text{cooling}} = \pi 0.049 d_1^{0.8} \mathcal{L} \quad (20)$$

$$\text{Minimum fraction heat lost} = \frac{0.021 \mathcal{L}}{R_1^{1.2}} \quad (21)$$

For an engine 100 feet long with an inlet radius of 20 feet, at least 6 percent of the energy added would be unavailable for propulsion in the ramjet example of the cycle analysis.

The problem of internal friction drag will not be considered, because this heat-transfer analysis clearly points out the desirability of small ratios of engine length to inlet radius. Designs minimizing internal heat losses will tend also to reduce the analogous friction-drag loss in the engine.

Discussion

Atmospheric models. - The Rocket Panel model atmosphere (table I) was assumed in the preceding analysis. Some consequences of this choice will now be discussed.

Despite the fact that both the cooling and drag problems decrease with increasing altitude, a low orbit altitude of about 60 miles was chosen for the example, because the kinetics of recombination are sensitive to total density and to the fraction of atomic oxygen. Since kinetics are theoretically the deciding factor in the engine efficiency, the ambient conditions for a desirable orbit would be high total density for short reaction times and a large fraction of atomic oxygen so that the recombination energy would provide appreciable temperature rise in the engine. Therefore, this brief discussion of the effect of the assumed atmospheric model on the cycle analysis is limited to the recombination problem at altitudes where the volume percentage of atomic oxygen is appreciable.

If table II had been used in the cycle analysis, the assumption of an orbit at least as high as 360,000 feet would have been necessary in order for an appreciable percentage of atomic oxygen to be present. The total density from table II at this altitude is about one-tenth that used in the supersonic-cycle analysis. If it is assumed that the engine has about the same ratio of inlet to throat area, then less than 10 percent of the oxygen can be expected to recombine in a 100-foot nozzle. Higher altitudes give less favorable results. Therefore, if a gradual transition region in percentage of atomic oxygen like that in table II should be confirmed by future research, a ramjet operating only on recombination energy probably would not be feasible.

The mass fraction of atomic oxygen at 328,080 feet in table III is very similar to that in table I. However, the ambient pressure and density of table III are about 20 percent smaller than the table I values at 328,080 feet. An estimate of the effect of these lower ambient conditions on recombination showed that about 50-percent recombination may still be possible in a 100-foot nozzle of an engine with a ratio of inlet to throat area of about 740, if k_p is 10^{13} (g-mole/liter)⁻²sec⁻¹

As a final comment, it should be emphasized that the crude kinetic analysis used in this report is justified only by the uncertainty in atmospheric composition and experimental rate data. When future research clarifies these uncertainties, then the cycle should be analyzed more exactly.

Alternative cycle. - A possible remedy for both the kinetic and cooling problems would be to inject a "third-body" gas into the flow at the throat. The injected gas would increase the effective density and

thus promote recombination in the nozzle. This scheme would detract from the fuelless feature but might make the engine operative at higher orbits. Furthermore, a gas-injection cycle would help solve the internal cooling problem, because the gas could be used in a regenerative cooling system. After cooling the internal surfaces, the hot gas could be injected into the flow to conserve energy lost by the closed-loop radiator scheme proposed for the fuelless cycle.

The problem with a gas-injection cycle is how to inject the gas into the supersonic flow efficiently. If there were shock losses due to injection, the engine efficiency would be lower than predicted for the supersonic cycle, but the added mass-flow rate in the nozzle would help counterbalance this loss. However, the engine would probably act as a good brake if a normal shock occurred at the gas-injection station.

CONCLUDING REMARKS

At every turn in this preliminary study, it has been necessary to make optimistic assumptions. Some of these assumptions concern future technology, and others concern facts of nature that are not yet known with certainty. Furthermore, this report has considered only the steady operation of the recombination ramjet in a circular orbit, and the problem of starting the supersonic inlet has not been discussed. The thermodynamic cycle analysis for an ideal engine with supersonic isentropic flow throughout and chemical-equilibrium nozzle flow indicated that sizable net thrusts could be realized (fig. 9). It would be possible to make allowances for inefficiencies due to internal heat transfer and drag, but the major assumption is equilibrium exhaust flow. Taking the preliminary results of an AVCO shock-tube experiment as the recombination-rate coefficient in the nozzle, there appears to be no chance for attaining chemical equilibrium in the expansion. However, sufficient recombination despite departure from equilibrium may be possible if engine lengths the order of 100 feet are used and if appreciable photochemical dissociation of air occurs at an altitude as low as 328,080 feet. However, drag and heat losses in internal cooling require that the ratio of length to inlet radius be kept as small as 5, or preferably smaller, for an engine 100 feet long.

An analysis of a recombination ramjet with normal-shock inlet and equilibrium nozzle flow showed that this cycle is not feasible.

Even though the recombination ramjet appears to be a marginal device, the problems of this engine do not appear impossible to solve if favorable atmospheric composition and reaction-rate coefficients are measured in future research. In that case, the fuelless ramjet could probably be developed for service where most of the lift is provided by the orbiting velocity.

Lewis Flight Propulsion Laboratory
National Advisory Committee for Aeronautics
Cleveland, Ohio, February 12, 1958

4780

CY-3 back

APPENDIX A

SYMBOLS

A	area, sq ft
\mathcal{A}	atom of "air"
C_D^i	form-drag coefficient for nonlift elements
C_{fr}	friction-drag coefficient
C_p	heat capacity of air at constant pressure
\mathcal{C}	concentration, g-mole/liter
D	total drag, lb(F)
D'	drag not due to lift, $D - D_L$, lb(F)
D_L	drag due to lift, lb(F)
d	diameter, ft
E	available energy, Btu/sec
e	available chemical-energy density, Btu/cu ft
F	thrust, lb(F)
\mathcal{E}_c	conversion factor, $\text{lb(M)ft}/\text{lb(F)sec}^2$
H	air enthalpy, Btu/lb(M)
\mathcal{H}	molar air enthalpy, Btu/lb-mole or cal/g-mole
$\Delta\mathcal{H}$	heat of reaction, appendix F
h	volumetric air enthalpy, Btu/cu ft
h_C	convective heat-transfer coefficient, $\text{Btu}/(\text{sec})(\text{sq ft})(^\circ\text{F})$, $\text{lb(M)}/(\text{sq ft})(\text{sec})$ in eq. (D1)
J	mechanical equivalent of heat, $\text{ft-lb(F)}/\text{Btu}$
K	chemical-equilibrium constant
K'	ratio of actual concentrations analogous to K, eq. (F9)
Kn	Knudsen number

k_F	recombination-rate coefficient, $(\text{g-mole/liter})^{-2}\text{sec}^{-1}$
k_r	dissociation-rate coefficient, $(\text{g-mole/liter})^{-2}\text{sec}^{-1}$
L	lift, lb(F)
\mathcal{L}	length of engine, ft
λ	mean free path of air
M	Mach number
\mathcal{M}	molecular weight
P	static pressure, lb(F)/sq ft
Pr	Prandtl number
q	heat-transfer rate, Btu/sec, eq. (11)
R	radius, ft
Re	Reynolds number
\mathcal{R}	universal gas constant
r	recovery factor
S	air entropy, Btu/lb(M) ^o R
St	Stanton number
T	absolute temperature
T'	lagging temperature (see appendix F)
t	time, sec
U	velocity, ft/sec
W	weight of aircraft, lb(F)
X	any air particle (atom or molecule)
x	length dimension
y_i	mass fraction of component i, $g(i)/g(\text{mixture})$
z	ratio of 28.97 to molecular weight of dissociated air

γ	ratio of specific heats
ϵ	emissivity
η	engine efficiency, eq. (C1)
θ	cone half-angle of nacelle (fig. 3)
κ	thermal conductivity of air
μ	air viscosity, lb(M)/(ft)(sec)
ρ	air density, lb(M)/cu ft, g/cc in appendix F
σ	Stefan-Boltzmann constant, 0.1713×10^{-8} Btu/(hr)(sq ft)($^{\circ}$ R) ⁴
τ	shear stress, lb(F)/ft

Subscripts:

aw	adiabatic wall
C	convective
\mathcal{C}	concentration
c	"combustion" chamber
e	equilibrium
F	frontal projected area of all external surfaces
f	forward reaction
f	film temperature
i	any component
N ₂	nitrogen
n	any nozzle station
O	atomic oxygen
O ₂	oxygen
R	radiation
r	reverse reaction

S solar
s surface
T temperature
w wall
X any air particle
y mass fraction
1 inlet conditions
2 throat or ambient to flat plate
3 exhaust-nozzle exit
 ∞ free stream

Superscripts:

- average
* reference conditions

APPENDIX B

COMPARISON OF TABULATED PHYSICAL PROPERTIES AND CHEMICAL-
ENERGY SOURCES OF UPPER ATMOSPHERE

From 1946 to 1955, over 200 rockets were fired in upper-atmospheric research, and more than half of these carried instruments for measuring the pressure and density of the atmosphere. Various authorities in upper-atmospheric physics have analyzed the accumulated data and have proposed tentative model atmospheres. The following discussion of the three atmospheric models presented in the text is included here for convenience. No implication as to the relative merits of the three model atmospheres is intended.

Tabulated Physical Properties

In 1955, pressure had been observed up to 425,000 feet, and density data extended to 725,000 feet. The probable errors in pressure and density were less than 10 percent at altitudes below 200,000 feet, but the errors increased with increasing altitude up to 200 to 300 percent at 660,000 feet (ref. 3).

Below 200,000 feet, the three atmospheric models of tables I to III agree within 10 percent. Above this altitude, the pressure and density of the three tables are difficult to compare, because no general trend persists over the entire altitude range. However, in the 300,000-foot region with which this report is primarily concerned, table I pressure and density are roughly 50 percent greater than table II values and about 20 percent greater than table III values. Reference 3 points out that a new set of density data was available in 1953 after the Rocket Panel had prepared its summary. Measurements of solar soft X-rays between 357,000 and 420,000 feet (ref. 14) indicated that the density in this region was lower than the average of previous experiments. Table II densities over this altitude range are the actual results of this experiment, while table III reflects these results with a smaller weighting.

The temperatures presented in all three tables were calculated from the perfect-gas law by assuming a mean molecular weight for air and using the given values of pressure and density. The mean molecular weight is determined by the chemical composition of air, and at present this composition is still an active research problem. Therefore, the variation in tabulated temperatures at very high altitudes is primarily the result of the different chemical compositions listed.

Tabulated Chemical Composition

The inert gases, which compose less than 3 percent of the atmosphere, are lumped into the tabulated percentage of nitrogen throughout this report.

Atmospheric ozone. - The vertical distribution of ozone from 30,000 to 230,000 feet has been measured directly five times with rockets equipped with spectrographs (ref. 3). The results are in good agreement with the vast amount of data on "total atmospheric ozone" collected by ground-level and balloon observations during the past 40 years. The averaged results of the rocket observations are given as table IV.

The averaged concentration data have a probable error of about 20 percent. Such excellent precision in measuring a "trace" component is due to the highly refined ultraviolet absorption technique employed. The sharp concentration peak at 100,000 feet is well established, and near this altitude ozone contributes significantly to the available chemical energy.

Gaseous ions. - Vertical distribution of electrons has been measured with high-altitude rockets, but physical theories of the ionosphere indicate that negative ions are also present (e.g., ref. 15). Therefore, the concentration of positive ions cannot be reliably inferred from electron densities. Apparently, ion densities have not been directly observed in rocket soundings. Furthermore, the energy of ionization might not be recoverable in a simple recombination-ramjet cycle. Since the ion density is uncertain, and the availability of ionization energy for thrust in a heat cycle is also questionable, the contribution of gaseous ions to the available chemical energy has been neglected throughout this report.

Atomic oxygen and nitrogen. - The only chemical constituents other than molecular oxygen and nitrogen that exist in sizable volume percentages in the atmosphere are atomic oxygen and nitrogen.

The Rocket Panel did not seriously propose that the composition of the atmosphere corresponds to that shown in table I above 260,000 feet. No data of chemical composition were available prior to 1952. However, in order to calculate temperature from the perfect-gas law using measured pressure and density, the Rocket Panel was forced to assume a mean molecular weight for air. Assuming that no dissociation occurred and that the molecular weight remained constant, they calculated the left temperature column of table I ($\bar{M} = 28.97$). Believing that these results were too high, the panel arbitrarily assumed a uniform dissociation rate for oxygen from zero at 262,464 feet (80 km) to complete dissociation at 393,696 feet (120 km), and similarly for nitrogen from zero dissociation at 393,696 feet to completion at 721,776 feet (220 km). The panel

4780

CY-4

presented the second column of temperature (table I, varying \bar{M}) as the "adopted value," emphasizing that they believed the dissociation assumptions were plausible.

An important set of composition data was obtained in conjunction with the total-density measurements from 357,000 to 420,000 feet in 1953 (ref. 14). A photon counter sensitive to molecular oxygen was also employed in these soundings with Aerobee rockets. The molecular oxygen particle density was measured directly throughout this altitude region. The percentage composition of atomic and molecular oxygen can be calculated from these measured molecular oxygen densities if both the total air density and the weight fraction of oxygen to nitrogen are known. Table II from 357,000 to 420,000 feet was constructed to correspond both to the total air and to the molecular oxygen densities observed in these 1953 flights, assuming the atmosphere would have been 21 volume-percent molecular oxygen if none were dissociated. However, Hulburt (ref. 3) points out that the total air density by X-ray measurements of 1953 "gave upper-air densities about 1/2 to 1/3 the values of table I in this altitude range. One cannot decide from the data at hand which is correct." For the composition below 357,000 feet, Hulburt used the atomic oxygen density results of a photochemical theory that accurately predicted the observed ozone density from 60,000 to 250,000 feet. Table IV summarizes these theoretical predictions, because atomic oxygen compositions smaller than 1 percent are not listed in table II. Above 420,000 feet, the composition given by table II is assumed. The particle densities of these constituents above 328,080 feet were calculated for equilibrium with gravity. The evidence for the dissociation of nitrogen was mainly theoretical.

As previously mentioned, the total densities in table III are slightly greater than the Hulburt-NRL values from 357,000 to 420,000 feet. Therefore, it is not surprising that the ARDC composition in this region differs slightly from that in table II, because higher density leads to a different interpretation of the Aerobee soundings. Below 357,000 feet, a more gradual transition in atomic oxygen was assumed in table III than in table II. Above 420,000 feet, table III composition parallels that of table II rather closely.

An interesting discussion of the 1953 Aerobee experiments has been published by the Ionosphere Research Group at Pennsylvania State College (e.g., ref. 16). The group presents an analysis that serves as a guide to extrapolating the experimental molecular oxygen density to higher altitudes.

Calculation of Available Chemical Energy

The following heats of formation were taken from reference 17:

Particles	Heat of formation, kcal/g-mole	
	at 0° K	at 298° K
Ozone, O ₃	-----	34.0
Atomic oxygen, O	-----	59.16
Atomic nitrogen, N	112.5	-----

The heat of formation is the change in enthalpy that would occur if molecular oxygen and nitrogen were converted to the listed particles at the given temperature. In these three cases, the energy associated with the reaction is very large compared with sensible-energy changes. For example, the heat of formation of atomic oxygen at 4000° K is 61.161 kilocalories per gram-mole, or only slightly greater than that listed for 298° K.

Until much better composition data are available, it is permissible to neglect the effect of temperature change with altitude and engine compression and to calculate the "available chemical energy" in the following manner. From table I, at an altitude of 459,312 feet,

Density, ρ, lb(M)/cu ft	4.747×10 ⁻¹⁰
Mean molecular weight, \bar{M} , lb/lb-mole "air"	21.21
Volume-percent atomic oxygen	30.7
Volume-percent atomic nitrogen	23.1

The total available chemical energy is equal to $\Delta h_{O_3} + \Delta h_O + \Delta h_N$:

$$\Delta h_{O_3} \approx 0 \text{ from table IV}$$

$$\begin{aligned} \Delta h_O &= \frac{30.7}{100.0} \times \frac{4.747 \times 10^{-10}}{21.21} \times 59.16 \times (453.6 \times 3.968) \\ &= 7.328 \times 10^{-7} \text{ Btu/cu ft} \end{aligned}$$

$$\begin{aligned} \Delta h_N &= \frac{23.1}{100.0} \times \frac{4.747 \times 10^{-10}}{21.21} \times 112.5 \times (453.6 \times 3.968) \\ &= 10.486 \times 10^{-7} \text{ Btu/cu ft} \end{aligned}$$

4780

.CY-4 back

Therefore, total available chemical energy is 1.78×10^{-6} Btu per cubic foot. This value is given in figure 1 at 450,000 feet for the Rocket Panel.

APPENDIX C

COMPARISON OF ENERGY AVAILABLE WITH ENERGY REQUIRED FOR FLIGHT

In this appendix some relations are developed to examine the flight spectrum permitted by the distribution of chemical energy in the atmosphere. Because the engine considered is a ramjet, only the lift-drag ratios for supersonic craft will be assumed. Only a rough treatment of drag is given here because of the cursory nature of this examination; these values are refined in the promising parts of the flight spectrum when the ionosphere ramjet is considered in detail in appendix D. The object of this analysis is to determine over what range of flight speed and altitude a ramjet using the chemical energy of the upper atmosphere can produce useful thrust.

The thrust of the ramjet engine can be written as

$$F = \frac{\eta EJ}{U_1} \quad (C1)$$

The lift-drag ratio L/D_L of the wing-fuselage combination in steady flight is

$$\frac{L}{D_L} = \frac{W}{F - D'} \quad (C2)$$

If the energy E is obtained from the intercepted atmosphere, it becomes

$$E = U_1 A_1 e \quad (C3)$$

Solving equations (C1), (C2), and (C3) for e yields

$$e = \frac{W}{A_1} \frac{D_L}{L} + \frac{D'}{A_1} \frac{1}{\eta J} \quad (C4)$$

The following breakdown of the nonlift drag terms will be used:

$$\frac{D'}{A_1} = C_D' \frac{A_F}{A_1} \frac{\rho_1 U_1^2}{2g_c} + \bar{C}_{fr} \frac{A_S}{A_1} \frac{\rho_1 U_1^2}{2g_c} = \bar{C}_{fr} \frac{P_1 \gamma M_1^2}{2} \left(\frac{C_D'}{\bar{C}_{fr}} \frac{A_F}{A_1} + \frac{A_S}{A_1} \right) \quad (C5)$$

where M_1 is the flight Mach number. As first approximations, let

$$\left. \begin{aligned} \frac{A_F}{A_1} &= 1 \\ \text{and} \\ \frac{A_S}{A_1} &= 10 \gg \frac{C_D'}{\bar{C}_{fr}} \end{aligned} \right\} \quad (C6)$$

A brief survey of current ramjet practice shows that the following assumptions are realistic:

$$\left. \begin{aligned} \frac{W}{A_1} &= 100 \frac{\text{lb(F)}}{\text{sq ft}} \\ \frac{L}{D_L} &= \frac{10}{1 - \frac{U_1^2}{Rg}} \end{aligned} \right\} \quad (C7)$$

where R is 2.112×10^7 feet, the approximate radius of the earth, and the gravitational constant g is 32.2 feet per second².

Equation (C4) can be simplified by using equations (C5) to (C7) as follows:

$$e = \frac{1}{\eta J} \left[10 \left(1 - \frac{U_1^2}{Rg} \right) + 5P_1 \gamma M_1^2 \bar{C}_{fr} \right] \quad (C8)$$

Equation (C8) gives the minimum energy density necessary to sustain flight in terms of the flight conditions and \bar{C}_{fr} .

The flow conditions in which the ramjet wing-fuselage will be flying must first be determined before the friction-drag coefficient is evaluated. Although the boundaries of slip and continuum flows are not sharply defined, the definitions of reference 18 will be adopted here. That is, the limit of continuum flow occurs where the Knudsen number ($Kn \equiv l/\mathcal{L}$) is less than 0.001, and slip flow exists for Kn from 0.001 to 2. If the characteristic length of the ramjet is 10 feet and the total length at least 100 feet, then the flow will be slip or continuum below about 425,000 feet. Furthermore, in the slip-flow region, \bar{C}_{fr} for continuum flow will probably be within 10 to 20 percent of the correct value (refs. 19 and 20). Therefore, \bar{C}_{fr} will be calculated from an empirical method that is applicable to continuum laminar flow.

The length average friction-drag coefficient for laminar flow over a flat plate is

$$\bar{C}_{fr} = \frac{1.328}{\sqrt{\frac{\rho U_1 x}{\mu}}} \quad (C9)$$

Eckert (refs. 6 and 7) has shown that, by evaluating the thermodynamic and physical properties of air at a defined reference temperature, equation (C9) can be used for a wide range of wall temperature and Mach number conditions. This calculation method is discussed in detail in appendix D; for approximate results, the reference-temperature method is convenient. The reference temperature for evaluating ρ and μ is defined as

$$T^* = 0.5(T_w + T_1) + 0.22(T_{aw} - T_1) \quad (C10)$$

where

$$T_{aw} = T_1 \left(1 + \frac{\gamma - 1}{2} r M_1^2 \right)$$

and

$$r = \frac{T_{aw} - T_1}{\frac{U_1^2}{2Jg_c C_p}}$$

It is convenient in this approximate analysis to use free-stream values of ρ and μ , designated by the subscript 1. Therefore, the effect of temperature on air properties is approximated by

$$\frac{\mu^*}{\mu_1} = \left(\frac{T^*}{T_1} \right)^{0.6}$$

and

$$\frac{\rho^*}{\rho_1} = \frac{T_1}{T^*}$$

so that

$$\frac{\rho^* U_1 x}{\mu^*} = \frac{\rho_1 U_1 x}{\mu_1} \left(\frac{T_1}{T^*} \right)^{1.6} \quad (C11)$$

Before the friction-drag coefficient determined by Eckert's method can be applied to this analysis, the definition for \bar{C}_{fr} by Eckert must

be reconciled with the definition used in equation (C5). That is, the reference-temperature method defines the average shearing stress $\bar{\tau}$ as

$$\left. \begin{aligned} \bar{\tau} &= \frac{1}{2} \bar{C}_{fr} \rho^* U_1^2 \\ \text{or} \\ \bar{\tau} &= \frac{1}{2} \bar{C}_{fr} \rho_1 U_1^2 \left(\frac{T_1}{T^*} \right) \end{aligned} \right\} \quad (C12)$$

However, in equation (C5) the implicit definition is

$$\bar{\tau} = \frac{1}{2} \bar{C}_{fr} \rho_1 U_1^2 \quad (C13)$$

The relation between the Eckert \bar{C}_{fr} in equation (C12) and the \bar{C}_{fr} for equation (C5) is simply

$$\bar{C}_{fr} \left(\frac{T_1}{T^*} \right) \Big|_{\text{eq. (C12)}} = \bar{C}_{fr} \Big|_{\text{eq. (C5)}} \quad (C14)$$

Combining equations (C9) and (C11) yields

$$\bar{C}_{fr} \Big|_{\text{eq. (C12)}} = \frac{1.328}{\sqrt{\frac{\rho_1 U_1 x}{\mu_1}}} \left(\frac{T_1}{T^*} \right)^{-0.8} \quad (C15)$$

Finally, the desired coefficient for equation (C5) results from substituting equation (C15) into (C14):

$$\bar{C}_{fr} \Big|_{\text{eq. (C5)}} = \frac{1.328}{\sqrt{\frac{\rho_1 U_1 x}{\mu_1}}} \left(\frac{T_1}{T^*} \right)^{0.2} \quad (C16)$$

Consider the friction-drag coefficient for two flight-speed conditions. Low supersonic Mach number:

$$\frac{T_1}{T^*} \approx 1 \quad (C17)$$

High supersonic Mach number: For orbital Mach number of about 23, $T_{aw}/T_1 = 1 + 0.2(550)$; and, assuming a material limit for the wall

temperature, $T_w/T_1 = 5$. Thus, equation (C10) can be evaluated as

$$\frac{T^*}{T_1} = 0.5(5 + 1) + 0.22(110) = 27.2$$

and

$$\left(\frac{T_1}{T^*}\right)^{0.2} \approx \frac{1}{2} \quad (C18)$$

Furthermore, it is assumed that

$$\frac{\rho_1 U_1 x}{\mu_1} = 10^2 \quad (C19)$$

Then, the \bar{C}_{fr} from equations (C17), (C19), and (C16) and from (C18), (C19), and (C16) are

$$\left. \begin{aligned} \bar{C}_{fr} &= 1.328 \times 10^{-2} \quad \text{for low Mach number} \\ \bar{C}_{fr} &= 0.664 \times 10^{-2} \quad \text{for high Mach number} \end{aligned} \right\} \quad (C20)$$

Finally, substitution of equation (C20) into equation (C8) gives

$$e = \frac{1}{\eta J} \left[10 \left(1 - \frac{U_1^2}{Rg} \right) + 5P_1 \gamma M_1^2 \left(1.328 \times 10^{-2} \text{ or } 0.664 \times 10^{-2} \right) \right] \quad (C21)$$

At low supersonic velocities and at high altitudes, the first term will dominate. Taking $\eta = 100$ percent,

$$e = \frac{10}{778} = 1.29 \times 10^{-2}$$

Comparison of this value with figure 1 shows that the atmosphere cannot provide the required energy anywhere.

For orbiting conditions, the first term of equation (C21) vanishes, and taking $\gamma = 1.4$ and $M_1 \approx 23$, the equation becomes

$$e = (3.27 \times 10^{-2}) P_1$$

Using table I densities and pressures together with figure 1, the following values are obtained:

Altitude, ft	Required e	Available e	
		Low	High
100,000	7.3×10^{-1}	4.0×10^{-5}	4.0×10^{-5}
300,000	1.4×10^{-4}	4.0×10^{-6}	9.0×10^{-5}
350,000	1.7×10^{-5}	3.0×10^{-6}	2.0×10^{-5}
400,000	2.9×10^{-6}	1.0×10^{-6}	5.0×10^{-6}
500,000	2.9×10^{-7}	1.0×10^{-7}	9.0×10^{-7}
600,000	4.9×10^{-8}	5.0×10^{-8}	2.0×10^{-7}

Thus, above 300,000 feet there is the possibility of obtaining thrust to overcome drag with an orbital ramjet that obtains its energy from the energized air it flies through. These values are for a Reynolds number of 10^4 . The influence of Reynolds number is discussed in the text under THE IONOSPHERE RAMJET.

APPENDIX D

HEAT TRANSFER AND FRICTION DRAG

By James F. Schmidt

Eckert's Laminar Heat-Transfer Theory for a Realistic Gas

Eckert's laminar flat-plate solution for the heat-transfer rate and skin-friction coefficient is applied herein to the three configurations shown in figure 3, a truncated cone, a circular cylinder, and a reversed truncated cone. Since large temperature variations are evident throughout the boundary layer at high speeds, Eckert's reference-enthalpy method is used rather than his reference-temperature method (refs. 6 and 7). This reference-enthalpy method accounts for the varying specific heat in boundary layers with large temperature variations.

The predominant reason for using Eckert's theory is that his approach is a direct calculation method that gives results comparable to those of methods that assume equilibrium dissociation of air (ref. 21). Reference 21 shows that the skin friction and heat transfer are relatively unaffected by dissociation if the surface temperature does not exceed 2500° R. In recent years some thought has been given to the phenomena of diffusion of dissociated particles. Some investigators have attempted to estimate the diffusion rates that could be used in heat-transfer calculations. However, sufficient information on diffusion rates is not available for such calculations at the present time.

All the heat-transfer calculations herein are based on the atmospheric properties of table I. The heat-transfer rate is defined as

$$q = h_c(H_{aw} - H_w) \quad (D1)$$

where H_w is the enthalpy due to wall temperature, and H_{aw} is the recovery enthalpy, defined as

$$H_{aw} = H_2 + r \left(\frac{U_2^2}{2g_c J} \right) \quad (D2)$$

where H_2 is the enthalpy due to the temperature of the gas surrounding the flat plate, and U_2 is the velocity of the gas relative to the flat plate. The recovery factor r is obtained from the following equation:

$$r = (Pr^*)^{1/2} \quad (D3)$$

4780

CY-5 back

where

$$\text{Pr}^* = \frac{\mu^* c_p^*}{\kappa^*} \quad (\text{D4})$$

A value of $\text{Pr}^* = 0.71$ is assumed in calculations for all configurations (ref. 7, fig. 3).

The reference enthalpy is calculated from the following semiempirical equation:

$$H^* = 0.5(H_w + H_2) + 0.22(H_{aw} - H_2) \quad (\text{D5})$$

The reference temperature is determined from the reference enthalpy. In the high-temperature range, a linear extrapolation of temperature against enthalpy from the gas tables of reference 22 is used. This linear extrapolation was checked against the tables of reference 23 for undissociated air up to 9000°R . Even at 9000°R the accuracy of the linear extrapolation is within 5 percent.

The skin-friction coefficient is given by the following equation:

$$C_{fr} = \frac{0.664}{\sqrt{\text{Re}^*}} = 0.664 \left(\frac{\mu^*}{\rho^* U_2 x} \right)^{1/2} \quad (\text{D6})$$

where

μ^* viscosity evaluated at reference temperature T^* ; formula for viscosity in NBS tables (ref. 23, p. 10) is used for all calculations

ρ^* density evaluated at reference temperature T^*

x length dimension of flat plate

The Stanton number is related to the friction coefficient by

$$\text{St} = \frac{C_{fr}}{2} (\text{Pr}^*)^{-2/3} \quad (\text{D7})$$

and

$$\text{St} = \frac{h_c}{\rho^* U_2} \quad (\text{D8})$$

Equilibrium External Wall Temperature

The equilibrium wall temperature is determined from the following energy balance equation:

$$q_C + q_S = q_R \quad (D9)$$

where

q_C convective heat-transfer rate to surface

q_S solar heat-transfer rate to surface

q_R radiation heat-transfer rate from surface

Convective heat-transfer rate. - Eckert's flat-plate solution is used for calculating the convective heat-transfer rates. The wall temperature has only a slight effect on the convective heat-transfer rate, primarily because the recovery temperature is extremely large in comparison with the relatively low wall temperature.

Solar heat-transfer rate. - The ramjet vehicle is assumed to be orbiting but not rotating, so that the sun radiates heat to only half the vehicle surface area at all times. In addition, the maximum heat energy is radiated to the ramjet by assuming that the sun's rays are always normal to the exposed surface area of the ramjet. Since the highest equilibrium wall temperature tends to produce the maximum external drag, the maximum heat energy transferred to the vehicle represents the worst flight condition.

The solar heat-transfer rates for the sunny and dark side of the vehicle are assumed to be 0.118 and 0 Btu/(sq ft)(sec), respectively. All the solar energy radiated to the vehicle surface is assumed to be completely absorbed. This assumption of complete absorption of the maximum amount of radiated solar heat energy predicts the largest external drag for all configurations.

Radiant heat-transfer rate. - The heat energy transferred away from the vehicle is assumed to be radiating to dark space. Therefore, this radiant heat-transfer rate is defined by the following equation:

$$q_R = \sigma \epsilon T_w^4 \quad (D10)$$

where the Stefan-Boltzmann constant σ is 0.1713×10^{-8} Btu/(hr)(sq ft)($^{\circ}\text{R}$)⁴, and the emissivity ϵ is taken as 1.0.

Equilibrium wall temperature against altitude. - A balance of energy between the convective plus the solar heat flux and the net radiation heat flux determines an equilibrium wall temperature (eq. (D9)). An equilibrium wall temperature was determined for the case in which all the energy of the atomic oxygen of the ambient air is assumed to be added to the free-stream energy. It is assumed that this condition would produce the highest equilibrium wall temperature for any given configuration. This high-energy condition was applied to configuration I (fig. 3(a)) with the following dimensions: a truncated cone with a 2° angle of inclination and a total length of 100 feet. A maximum equilibrium wall temperature of slightly less than 1000° R was calculated for configuration I. The combination of these dimensions for configuration I and the high-energy condition is believed to give the highest possible equilibrium wall temperature.

In order to ensure more than marginal safety, a wall temperature of 1000° R is assumed for all drag calculations. Since configuration III appears to give the lowest external drag, an equilibrium wall temperature was calculated for this configuration at 328,000 feet. This calculated temperature was found to be more than 300° R lower than the assumed value of 1000° R. Therefore, it is evident that the assumed wall temperature of 1000° R is conservative.

Also, the effect of altitude on wall temperature is negligible for altitudes up to 700,000 feet (fig. 11).

External Surface Drag Per Inlet Area

Surface drag per inlet area for configuration I in continuum flow. - An oblique shock wave is produced at the inlet of the truncated cone (fig. 3). The flow properties behind the shock are found from oblique-shock-wave theory (ref. 24) for a perfect gas using free-stream conditions. The skin-friction coefficient is calculated as a function of the flat-plate length x by use of Eckert's flat-plate solution with the flow properties behind the oblique shock wave. The truncated cone is treated as a flat plate with infinitesimal width at an angle of attack. Expressing the surface area of the cone as a function of x , the surface drag is obtained by integrating the product of the local friction drag and the unit surface area over the surface length of the cone. This drag is divided by the inlet area in order to give the external surface drag per inlet area:

$$D = \int_0^L \tau_w dA_s \quad (D11)$$

where

$$dA_s = f(x) = 2\pi(R_1 + x \tan \theta)dx \quad (D12)$$

$$\tau_w = \frac{C_{fr}\rho^*U_2^2}{2g_c} \quad (D13)$$

and

$$C_{fr} = f(x) \quad (D14)$$

Therefore, the surface drag per inlet area is

$$\frac{D}{A_1\rho_1} = \frac{\rho^*U_2^2}{g_c R_1^2 \rho_1} \int_0^{\mathcal{L}} C_{fr}(R_1 + x \tan \theta)dx \quad (D15)$$

The pressure drag has negligible effect on the total surface drag for this configuration with small cone angles. All drag calculations are based on the atmospheric properties of table I.

Surface drag per inlet area for configuration II in continuum flow. - Since configuration II, a circular cylinder, as shown in figure 3 is orientated at 0° to the free-stream flow direction, no shock waves will occur on the cylinder. Hence, free-stream flow properties are used in Eckert's flat-plate solution for the skin-friction coefficient.

The circular cylinder is treated in the same manner as the truncated cone (configuration I) for obtaining the surface drag per inlet area (eq. (D11)), where

$$dA_s = f(x) = 2\pi R_1 dx \quad (D16)$$

and equations (D13) and (D14) apply.

Hence, the surface drag per inlet area becomes

$$\frac{D}{A_1\rho_1} = \frac{\rho^*U_2^2}{g_c R_1 \rho_1} \int_0^x C_{fr} dx \quad (D17)$$

Surface drag per inlet area for configuration III in continuum flow. - A Prandtl-Meyer expansion is produced at the inlet of the reversed truncated cone (fig. 3). Since the expansion angle is small ($\theta = -4.3^\circ, -8.617^\circ$), the two-dimensional Prandtl-Meyer expansion is assumed to be a good approximation for the flow around the corner of the cone.

Using the properties behind the Prandtl-Meyer expansion in Eckert's flat-plate solution, the skin-friction coefficient is calculated as a function of the flat-plate length x . The reversed truncated cone is also treated in the same manner as the truncated cone for calculating the surface drag per inlet area (eqs. (D11) to (D15)). The pressure drag for this configuration is neglected, because it actually produces a negligible force in the thrust direction.

Maximum Internal Heat-Transfer Rate

The maximum internal heat-transfer rate is encountered at the throat of the ramjet nozzle. The internal heat-transfer calculation was made for configuration III with the following geometric dimensions:

$$\theta = -8.616^\circ$$

$$\mathcal{L} = 100 \text{ ft}$$

$$\frac{\mathcal{L}}{R_1} = 5$$

$$d_1 = 40 \text{ ft}$$

$$\frac{A_1}{A_2} = 740.65$$

$$d_2 = 0.465 \text{ ft}$$

The heat-transfer rate is defined by the following equation:

$$q = h_C(T_{aw} - T_w) \quad (D18)$$

The following values were assumed: Allowable wall temperature with maximum internal cooling T_w , 1660° R, and adiabatic temperature of the dissociated air T_{aw} , 9850° R.

The heat-transfer coefficient h_C (ref. 13) is determined from

$$h_C = \frac{x_f}{d_2} (0.023) \left(\frac{d_2 \rho_2 U_2}{\mu_f} \right)^{0.8} \left(\frac{C_p \mu}{x} \right)_f^{0.33} \quad (D19)$$

where the film temperature T_f is 3311° R, and

$$x_f = 174.5 \times 10^{-7} \text{ Btu}/(\text{ft})(\text{sec})(^\circ\text{R})$$

$$\rho_2 = 410 \times 10^{-7} \text{ lb/cu ft}$$

$$U_2 = 24,743 \text{ ft/sec}$$

$$\mu_f = 419 \times 10^{-7} \text{ lb/(sec)(ft)}$$

$$(C_p \mu / \kappa)_f = \text{Pr} = 0.71$$

The resulting heat-transfer rate is

$$\frac{q}{A_s} = 10.82 \text{ Btu/(sec)(sq ft)}$$

4780

CY-6

APPENDIX E

NORMAL-SHOCK ORBITING RAMJET CYCLE

The all-supersonic ramjet cycle discussed in the text gives ideal engine efficiencies up to 85 percent. However, since the problem of starting such a ramjet might be great, it is natural to investigate cycles involving inlet shocks. The extreme case of a normal-shock inlet will be examined here. The lower engine velocities would give longer, more favorable reaction times; and, as outlined in appendix F, the recombination kinetics would be a critical problem.

For this example, the flight altitude and velocity are identical with those of the all-supersonic cycle. The problem is twofold: (1) The flow conditions after shock must be determined, and (2) the cycle must be completed by expanding the air to ambient pressure and obtainable thrust must be calculated.

The flow immediately following the normal shock will not be in chemical equilibrium, because even dissociation kinetics are relatively slow at these rarified gas conditions. However, the air after shock will approach equilibrium if isentropic constant-area flow sufficient for reaction is assumed to exist downstream. This assumption is made in the following analysis.

The following four equations must be satisfied at the inlet:

Continuity:

$$\rho_{\infty} U_{\infty} = \rho_1 U_1 \quad (E1)$$

Conservation of momentum:

$$P_1 - P_{\infty} = \frac{1}{g_c} (\rho_{\infty} U_{\infty}^2 - \rho_1 U_1^2) \quad (E2)$$

Conservation of energy:

$$2g_c J(H_1 - H_{\infty}) = U_{\infty}^2 - U_1^2 \quad (E3)$$

Equation of state:

$$P_1 = \mathcal{R} z_1 \rho_1 T_1 \quad (E4)$$

The subscript ∞ refers to the free-stream conditions, and 1 is the inlet or after-shock flow. The solution of these equations is straightforward, but it involves a trial-and-error procedure and the use of

charts of thermodynamic properties of dissociated air. The known free-stream conditions are identical with those for the all-supersonic ramjet cycle used in the text:

$$U_{\infty} = 26,050 \text{ ft/sec}$$

$$\rho_{\infty} = 5.375 \times 10^{-8} \text{ lb(M)/cu ft}$$

$$P_{\infty} = 1.24 \times 10^{-3} \text{ lb(F)/sq ft}$$

$$H_{\infty} = 984.8 \text{ Btu/lb(M)}$$

$$z_{\infty} = 1.103$$

Briefly, the calculation procedure is to use an assumed U_1 in a combination of equations (E1) and (E2) and also in equation (E3). Furthermore, it is assumed that the air after shock is in chemical equilibrium, so that the calculated P_1 and H_1 determine T_1 and z_1 on a Mollier chart for air (ref. 8). Equation (E4) with the determined values of z_1 , T_1 , and P_1 yields the corresponding ρ_1 . Finally, this procedure is repeated until the continuity equation (E1) is satisfied by the assumed U_1 and the calculated ρ_1 . In this manner, the flow conditions after shock were found to be

$$U_1 = 1195 \text{ ft/sec}$$

$$P_1 = 1.13 \text{ lb(F)/sq ft}$$

$$\rho_1 = 1.17 \times 10^{-6} \text{ lb(M)/cu ft}$$

$$T_1 = 9630^{\circ} \text{ R}$$

$$z_1 = 1.888$$

$$H_1 = 14,400 \text{ Btu/lb(M)}$$

$$\frac{\bar{M}_1 S_1}{R} = 65.55$$

The remainder of the cycle is easily determined on the Mollier chart by following the isentropic curve $\bar{M}_1 S_1 / R$ to ambient pressure or P_{∞} .

Though the chart used did not extend over the entire pressure range, a crude extrapolation is sufficient; this will be evident after the thrust calculation.

The nozzle exhaust properties by extrapolation are

$$T_3 = 3650(1.8) \text{ } ^\circ\text{R}$$

$$H_3 = 7250 \text{ Btu/lb(M)}$$

$$z_3 = 1.45$$

From the energy equation and continuity,

$$U_3 = 18,950 \text{ ft/sec}$$

$$\frac{A_3}{A_\infty} = 30.1$$

The thrust from this normal-shock-inlet cycle was calculated from

$$\frac{F}{A_\infty} = \frac{\rho_\infty U_\infty}{g_c} (U_3 - U_\infty) + P_3 \left(\frac{A_3}{A_\infty} \right) - P_\infty \quad (9)$$

$$= -10 \text{ lb(F)/sq ft}$$

This large drag clearly reflects not only the inefficiency of a shock cycle but also the fact that the great dissociation at the extreme inlet temperature cannot be recovered in the exhaust nozzle to any appreciable extent.

APPENDIX F

CHEMICAL KINETICS OF RECOMBINATION

The first two sections of this appendix apply the general method of reference 10 to the recombination of atomic oxygen in an adiabatic nozzle flow. An equation that is used as a criterion for near-equilibrium flow is obtained first, and then a similar relation is obtained for near-frozen expansion. In the final section, these limiting cases are considered in a numerical example to point out the necessary kinetic conditions on the thermodynamic cycle assumptions.

Adiabatic Expansion with Near-Equilibrium Flow

The intuitive meaning attached to "near-equilibrium flow" is that the difference between the actual weight fractions of a given chemical component y_i and the equilibrium weight fractions for the local conditions of temperature and pressure $y_{i,e}$ is not large. Before stating the precise definition, it will be necessary to review some background thermodynamic and kinetic equations. Then, a useful criterion for near-equilibrium flow will be reduced from a mathematical formulation of the preceding qualitative statement.

For this analysis, let the actual molecular reaction be



The rate of the forward recombination reaction is given by

$$k_f \mathcal{C}_O^2 \mathcal{C}_X \quad (F2)$$

where \mathcal{C}_i is the concentration of species i (g-mole(i)/cc) and the subscript O refers to atomic oxygen and X to all "third bodies," taken here as the total molar density. This expression assumes isothermal constant-volume reaction. Similarly, the dissociation rate is

$$k_r \mathcal{C}_{O_2} \mathcal{C}_X \quad (F3)$$

where the subscript O_2 refers to molecular oxygen.

The net production rate of atomic and molecular oxygen in the reversible reaction equation (F1) can be written in terms of equations (F2) and (F3) as

$$-\frac{1}{2} \frac{d\mathcal{C}_O}{dt} = \frac{d\mathcal{C}_{O_2}}{dt} = k_F \mathcal{C}_O^2 \mathcal{C}_X - k_R \mathcal{C}_{O_2} \mathcal{C}_X \quad (\text{F4})$$

The factor 1/2 is determined by the stoichiometry of the reaction; two moles of atomic oxygen react for every mole of molecular oxygen formed.

Later in this analysis, it will be convenient to work with the continuity equation in terms of weight fractions rather than molar concentrations. Therefore, noting that

$$\mathcal{C}_i = \frac{y_i \rho}{M_i} \quad (\text{F5})$$

where

y_i weight fraction species i , $g(i)/g(\text{mixture})$

ρ total mass density, $g(\text{mixture})/cc$

M_i molecular weight of i , $g(i)/g\text{-mole}(i)$

equation (F4) is rewritten:

$$\frac{d\mathcal{C}_{O_2}}{dt} = -\frac{1}{2} \frac{d\mathcal{C}_O}{dt} = k_F \frac{\rho^3}{M_O^2 M_X} y_O^2 y_X - k_R \frac{\rho^2}{M_{O_2} M_X} y_{O_2} y_X \quad (\text{F6})$$

At this point, the thermodynamic chemical equilibrium constant at the local temperature and total pressure can be introduced. Defining the equilibrium constant in terms of equilibrium concentrations in the usual manner and then using equation (F5) to obtain its relation to an equilibrium constant in weight fractions give

$$\left. \begin{aligned} K_{\mathcal{C}} &= \frac{(\mathcal{C}_{O_2})_e}{(\mathcal{C}_O)_e^2} \\ K_y &= \frac{(y_{O_2})_e}{(y_O)_e^2} \\ K_{\mathcal{C}} &= \frac{M_O^2}{M_{O_2}} \frac{1}{\rho} K_y \end{aligned} \right\} \quad (\text{F7})$$

The subscript e denotes that equilibrium values must be used. Furthermore, at equilibrium the net rate of production of all chemical species is zero. Thus,

$$K_{\mathcal{C}} = \frac{k_f}{k_r} = \frac{(\mathcal{C}_{O_2})_e}{(\mathcal{C}_O)_e^2} \tag{F8}$$

Equation (F6) can be written in terms of k_f and $K_{\mathcal{C}}$ by using equation (F8). However, before doing this, it is convenient to define a term analogous in form to the equilibrium constant but expressed in terms of the actual weight fractions at the local temperature and pressure:

$$\left. \begin{aligned} K'_{\mathcal{C}} &= \frac{\mathcal{C}_{O_2}}{\mathcal{C}_O^2} \\ K'_y &= \frac{y_{O_2}}{y_O^2} \\ K'_{\mathcal{C}} &= \frac{\mathcal{M}_O^2}{\mathcal{M}_{O_2}} \frac{1}{\rho} K'_y \end{aligned} \right\} \tag{F9}$$

Substituting equations (F8) and (F9),

$$\frac{d\mathcal{C}_{O_2}}{dt} = -\frac{1}{2} \frac{d\mathcal{C}_O}{dt} = k_f \frac{\rho^3}{\mathcal{M}_O^2 \mathcal{M}_X} y_{O_2}^2 y_X \left(1 - \frac{K'}{K} \right) \tag{F10}$$

Note that the subscript has been dropped from K'/K , because from equations (F7) and (F9) it is apparent that $\frac{K'_{\mathcal{C}}}{K_{\mathcal{C}}} = \frac{K'_y}{K_y} = \frac{K'}{K}$.

Reference 10 shows that a one-dimensional-flow continuity equation for negligible diffusion currents is

$$\frac{D \ln y_{O_2}}{Dt} - 2 \frac{D \ln y_O}{Dt} = \frac{1}{\mathcal{C}_{O_2}} \frac{d\mathcal{C}_{O_2}}{dt} - 2 \frac{1}{\mathcal{C}_O} \frac{d\mathcal{C}_O}{dt} \tag{F11}$$

where the Euler total derivative for steady x-direction flow is

$$\frac{D}{Dt} = U \frac{d}{dx}$$

4780

A coordinate transformation on the left side of equation (F11) introduces the time rate of change of temperature T :

$$\left(\frac{d \ln y_{O_2}}{dT} - 2 \frac{d \ln y_O}{dT} \right) \frac{DT}{Dt} = \frac{1}{\mathcal{C}_{O_2}} \frac{d\mathcal{C}_{O_2}}{dt} - 2 \frac{1}{\mathcal{C}_O} \frac{d\mathcal{C}_O}{dt} \quad (F12)$$

The desired equation for developing criteria for near-equilibrium flow and for near-frozen flow is obtained by combining equations (F9), (F10), and (F12):

$$\left(\frac{d \ln K'_y}{dT} \right)_T = \left(\frac{DT}{Dt} \right)^{-1} k_{fp}^2 \left[\left(\frac{y_O}{\mathcal{M}_O} \right)^2 \left(\frac{y_X}{\mathcal{M}_X} \right) \left(1 - \frac{K'}{K} \right) \right] \left(\frac{\mathcal{M}_{O_2}}{y_{O_2}} + \frac{4\mathcal{M}_O}{y_O} \right) \quad (F13)$$

The statement at the beginning of this analysis indicated that in near-equilibrium flow the difference between y_i and $y_{i,e}$ is not large. Following Penner, the quantity K'_y can be considered to be an equilibrium constant at a temperature T' that is slightly different from the actual local temperature T . The precise definition for near-equilibrium flow states that the temperature difference " $T' - T$ " is so small that it is sufficient to retain only the first two terms in the Taylor series expansion of $K'_y = K_y(T')$ about the temperature T (ref. 10). That is, for near-equilibrium flow,

$$K'_y = K_y(T') \approx K_y(T) + K_y(T) \left[\frac{d \ln K_y(T)}{dT} \right] (T' - T) \quad (F14)$$

Equation (F14) is easily rearranged to

$$1 - \frac{K'_y}{K_y} = - \left[\frac{d \ln K_y(T)}{dT} \right]_T (T' - T) \quad (F15)$$

Equation (F15), along with the approximation that $\left(\frac{d \ln K'_y}{dT} \right)_T \approx \left[\frac{d \ln K_y(T)}{dT} \right]_T$, is now substituted into equation (F13), which simplifies to the following equation in terms of molar concentrations:

$$T' - T \approx \left(- \frac{DT}{Dt} \right) \left[k_{fp} \mathcal{C}_X \left(4\mathcal{C}_O + \frac{\mathcal{C}_O^2}{\mathcal{C}_{O_2}} \right) \right]^{-1} \quad (F16)$$

Equation (F16) relates the temperature lag associated with the composition of the near-equilibrium reacting gas mixture to the temperature rate of change with time at a given point in the exhaust and a reaction time (in parentheses).

Adiabatic Expansion with Near-Frozen Flow

Penner (ref. 10) defines near-frozen flow as flow for which the extent of chemical reaction is so small that the difference $T_c - T'$ always remains small. Here, T_c is the temperature of the gas at the start of expansion; and, as in near-equilibrium flow, T' is a temperature for which $K_y(T') = K_y'$. Therefore, in this case the criterion is

$$K_y' = K_y(T') \approx K_y(T_c) - K_y(T_c) \left[\frac{d \ln K_y(T)}{dT} \right]_{T_c} (T_c - T') \quad (F17)$$

Equation (F13) can be written in terms of molar concentrations as equation (F18) by solving equation (F17) for $\left[\frac{d \ln K_y(T)}{dT} \right]_{T_c}$ and using the approximation that

$$\left(\frac{d \ln K_y}{dT} \right)_T \approx \left[\frac{d \ln K_y(T)}{dT} \right]_{T_c} \frac{T_c - T'}{T_c - T}$$

That is,

$$\begin{aligned} \frac{T_c - T'}{T_c - T} &= \left(- \frac{DT}{Dt} \right)^{-1} k_f \mathcal{E}_X \left(4\mathcal{E}_O + \frac{\mathcal{E}_O^{-2}}{\mathcal{E}_{O_2}} \right) \left(- \frac{d \ln K_y}{dT} \right)_{T_c}^{-1} \left[1 - \frac{K_y(T_c)}{K_y(T)} \right] \\ &+ \left(- \frac{DT}{Dt} \right)^{-1} k_f \mathcal{E}_X \left(4\mathcal{E}_O + \frac{\mathcal{E}_O^2}{\mathcal{E}_{O_2}} \right) \frac{K_y(T_c)}{K_y(T)} (T_c - T') \end{aligned} \quad (F18)$$

This equation can be reduced by noting that, in the numerical example being considered, $\frac{K_y(T_c)}{K_y(T)} \ll 1$ and that $T_c - T'$ is also small, so that equation (F18) simplifies to the following:

$$\frac{T_c - T'}{T_c - T} \approx \left(- \frac{DT}{Dt} \right)^{-1} k_f \mathcal{E}_X \left(4\mathcal{E}_O + \frac{\mathcal{E}_O^2}{\mathcal{E}_{O_2}} \right) \left(- \frac{d \ln K_y}{dT} \right)_{T_c}^{-1} \quad (F19)$$

4780

4780

Chemical thermodynamics can be used to express the temperature-dependence of the weight-fraction equilibrium constant K_y in terms of the heat of the oxygen recombination reaction $\Delta \mathcal{H}$. The exact form of this relation is complicated, but the following equation is a good approximation:

$$\frac{d \ln K_y}{dT} = \frac{\Delta \mathcal{H}}{\mathcal{R} T^2} \quad (\text{F20})$$

Therefore, equation (F18) can be written as

$$\frac{T_c - T'}{T_c - T} = \left(- \frac{DT}{Dt} \right)^{-1} k_f \mathcal{C}_X \left(4 \mathcal{C}_O + \frac{\mathcal{C}_O^2}{\mathcal{C}_{O_2}} \right) \frac{\mathcal{R} T_c^2}{-\Delta \mathcal{H}} \quad (\text{F21})$$

Equation (F21) is the desired expression for characterizing near-frozen-composition expansion.

Numerical Example

Before applying equations (F16) and (F21) to the nozzle example of the cycle analysis, two basic assumptions should be pointed out. The most important is the assumption that the reaction-rate coefficient k_f is not temperature-dependent. In general, chemical reaction rates are very temperature-sensitive. However, for the recombination reaction given by equation (F1) (forward reaction), only an algebraic temperature-dependence should be expected if oxygen recombination follows the trend observed in iodine atomic recombination and hydrogen atomic recombination. In the latter two reactions, near-zero activation energies have been observed. For lack of sufficient data the k_f has been assumed to be temperature-independent. Secondly, the total derivative DT/Dt is assumed to be constant throughout the nozzle; this is an adequate approximation for the limiting cases being considered.

Near-equilibrium expansion. - The temperature, pressure, and composition conditions in the equilibrium expansion cycle calculation are used here. Specifically,

$$- \frac{DT}{Dt} = - U \frac{dT}{dx} = \bar{U} \left(\frac{T_2 - T_3}{\mathcal{L}} \right)$$

assuming that

$$\mathcal{L} = 100 \text{ feet}$$

$$\bar{U} = 25,000 \text{ ft/sec}$$

$$-\frac{DT}{Dt} = 5.5 \times 10^5 \text{ } ^\circ\text{K/sec}$$

The molar concentrations of O, O₂, and X (total) are calculable from the equilibrium nozzle conditions given by figures 5 and 6. By assigning a maximum temperature lag (T' - T), equation (F16) was solved for minimum values of k_f. The results of this calculation using T' - T ≤ 20° K are given in table V. This temperature lag is somewhat arbitrary, but an examination showed that 20° K is small enough to assure the rapid convergence of the Taylor series (eq. (F14)) for the oxygen recombination reaction.

Near-frozen expansion. - The calculation procedure for near-frozen expansion is identical to that for near-equilibrium expansion, except that $\left(\frac{T_c - T'}{T_c - T}\right) \leq 10^{-2}$ was used in equation (F21) to calculate the maximum k_f possible before the flow deviates from frozen expansion. The heat of reaction given in appendix B (Δℋ = 2(59,160) cal/mole O₂) and T_c = T₂ = 2763° K are the additional information required. The results of these calculations are also given in the text. The reduced temperature ratio of 10⁻² is sufficient for the convergence of the Taylor series (eq. (F17)) to within 10 percent in two terms.

An apparent inconsistency in the derivation of equation (F21) and its application in this example should be pointed out and explained. The derivation assumes that the gas at the start of expansion is in chemical equilibrium; this justifies the use of equation (F20). The results of this crude analysis, as discussed in the text, show that equilibrium flow may never be attained in the example nozzle. However, from figure 6, it is apparent that in this cycle the difference between the ambient frozen composition and the equilibrium composition at T₂ and P₂ is very slight, being off only by the presence of 2 percent nitric oxide at equilibrium. Therefore, the use of equation (F21) appears justifiable in this example.

Percent recombined. - The molar concentrations of atomic oxygen corresponding to the necessary ℳ₀ for a given k_f and flow condition can easily be related to the degree of recombination in the nozzle. Since the pressure and temperature change markedly in the nozzle, the percentage recombination is defined here in mass units:

$$\text{Percent recombined} = 100 \left[\frac{(y_O)_2 - (y_O)_n}{(y_O)_2} \right] \quad (\text{F22})$$

This equation can be rewritten in terms of the molar concentrations at stations 2 and any other nozzle condition n :

$$\text{Percent recombined} = 100 \left[1 - \frac{\bar{M}_2 (\mathcal{C}_O)_n (\mathcal{C}_X)_2}{\bar{M}_n (\mathcal{C}_O)_2 (\mathcal{C}_X)_n} \right] \quad (\text{F23})$$

The nozzle conditions summarized in figures 5 and 6 were used in equation (F23) to calculate figure 10.

REFERENCES

1. Proell, Wayne: The Significance of Monatomic Gases in Planetary Space Operations. The Jour. Space Flight, Chicago, vol. 2, no. 7, Sept. 1950, pp. 1-8; pt. 2, vol. 2, no. 8, Oct. 1950, pp. 1-9.
2. The Rocket Panel: Pressure Densities and Temperatures in the Upper Atmosphere. Phys. Rev., vol. 88, no. 5, Dec. 1, 1952, pp. 1027-1032.
3. Hulburt, E. O.: Advances in the Physics of the Upper Air Since 1950. Rep. 4600, NRL, Oct. 25, 1955.
4. Minzner, R. A., and Ripley, W. S.: The ARDC Model Atmosphere, 1956. TN-56-204, Geophys. Res. Directorate, AF Cambridge Res. Center, Air Res. and Dev. Command, Dec. 1956. (ASTIA Doc. 110233.)
5. Anon.: Atmospheric Models. Doc. No. 56SD233, Missile and Ord. Systems Dept., General Electric Co., 1956.
6. Eckert, E. R. G.: Engineering Relations for Heat Transfer and Friction in High-Velocity and Turbulent Boundary-Layer Flow over Surfaces with Constant Pressure and Temperature. Trans. ASME, vol. 78, no. 6, Aug. 1956, pp. 1273-1283.
7. Eckert, Ernst R. G.: Survey on Heat Transfer at High Speeds. Tech. Rep. 54-70, Aero. Res. Lab., Apr. 1954. (Contract AF 33(616)-2214.)
8. Hilsenrath, Joseph, and Beckett, Charles W.: Thermodynamic Properties of Argon-Free Air (0.78847N₂, 0.21153O₂) to 15,000° K. Rep. 3991, NBS, Apr. 1, 1955. (See also NACA TN 4265.)
9. Gordon, Sanford, and Glueck, Allan R.: Theoretical Performance of Liquid Ammonia with Liquid Oxygen as a Rocket Propellant. NACA RM E58A21, 1958.

10. Penner, S. S.: Introduction to the Study of Chemical Reactions in Flow Systems. AGARDograph 7, Butterworth Sci. Pub. (London), 1955.
11. Frost, Arthur A., and Pearson, Ralph G.: Kinetics and Mechanism. John Wiley & Sons, 1953, p. 104.
12. Feldman, Saul: The Chemical Kinetics of Air at High Temperature: A Problem in Hypersonic Aerodynamics. Rep. no. 4, AVCO Res. Lab., Feb. 1957. (Contract AF 04(645)-18.)
13. Sutton, George P.: Rocket Propulsion Elements. Second ed., John Wiley & Sons, Inc., 1956, p. 134.
14. Byram, E. T., Chubb, T. A., and Friedman, H.: Dissociation of Oxygen in the Upper Atmosphere. Phys. Rev., vol. 98, no. 6, June 15, 1955, pp. 1594-1597.
15. Mitra, A. P.: Night-Time Ionization in the Lower Ionosphere. II - Distribution of Electrons and Positive and Negative Ions. Jour. Atmospheric and Terrestrial Phys., vol. 10, no. 3, Mar. 1957, pp. 153-162.
16. Mange, P.: The Diffusion and Dissociation of Molecular Oxygen in the Atmosphere Above 100 km. Rep. No. 64, Ionosphere Res. Lab., The Penn. State Univ., June 15, 1954. (Contract AF 19(122)-24.)
17. Rossini, Frederick D., et al.: Selected Values of Chemical Thermodynamic Properties. Cir. 500, NBS, Feb. 1952.
18. Stalder, Jackson R., Goodwin, Glen, and Creager, Marcus O.: Heat Transfer to Bodies in a High-Speed Rarefied-Gas Stream. NACA Rep. 1093, 1952. (Supersedes NACA TN 2438.)
19. Mirels, Harold: Estimate of Slip Effect on Compressible Laminar-Boundary-Layer Skin Friction. NACA TN 2609, 1952.
20. Maslen, Stephen H.: Second Approximation to Laminar Compressible Boundary Layer on Flat Plate in Slip Flow. NACA TN 2818, 1952.
21. Moore, L. L.: A Solution of the Laminar Boundary-Layer Equations for a Compressible Fluid with Variable Properties, Including Dissociation. Jour. Aero. Sci., vol. 19, no. 8, Aug. 1952, pp. 505-518.
22. Keenan, Joseph H., and Kaye, Joseph: Gas Tables - Thermodynamic Properties of Air Products of Combustion and Component Gases. John Wiley & Sons, Inc., 1950.

23. Hilsenrath, Joseph, et al.: Tables of Thermal Properties of Gases. Cir. 564, NBS, Nov. 1, 1955.
24. Ames Research Staff: Equations, Tables, and Charts for Compressible Flow. NACA Rep. 1135, 1953. (Supersedes NACA TN 1428.)

TABLE I. - ROCKET RESEARCH PANEL; ADOPTED ATMOSPHERIC DATA (REF. 2)

[Converted to engineering units.]

Altitude (above sea level), ft (b)	Physical properties				Chemical composition ^a					
	Temp. for $\rho = 28.97$, °F	Pressure, lb(F)/sq ft	Density, lb(M)/cu ft	Temp. for varying ρ , °F	Mean molecular weight, M , lb/lb-mole	Volume percent O ₂	Volume percent O	Volume percent N ₂	Volume percent N	Weight ratio, Oxygen Nitrogen
3,989	64.1	1840	6.582X10 ⁻²	64.1	28.97	21	0	79	0	0.5020
15,125	31.0	1316	5.018X10 ⁻²	31.0	28.97	21	0	79	0	.5020
28,248	-18.7	777.7	3.307X10 ⁻²	-18.7	28.97	21	0	79	0	.5020
39,370	-54.8	431.4	2.048X10 ⁻²	-54.8	28.97	21	0	79	0	.5020
52,493	-85.3	227.4	1.159X10 ⁻²	-85.3	28.97	21	0	79	0	.5020
85,616	-76.7	118.8	6.826X10 ⁻³	-76.7	28.97	21	0	79	0	.5020
78,740	-62.1	83.66	5.002X10 ⁻³	-62.1	28.97	21	0	79	0	.5020
91,863	-48.4	54.82	1.590X10 ⁻³	-48.4	28.97	21	0	79	0	.5020
104,986	-35.6	19.45	8.598X10 ⁻⁴	-35.6	28.97	21	0	79	0	.5020
118,110	-15.1	11.11	4.871X10 ⁻⁴	-15.1	28.97	21	0	79	0	.5020
151,232	12.8	8.559	2.802X10 ⁻⁴	12.8	28.97	21	0	79	0	.5020
144,358	27.2	5.961	1.525X10 ⁻⁴	27.2	28.97	21	0	79	0	.5020
157,480	29.2	2.409	8.255X10 ⁻⁵	29.2	28.97	21	0	79	0	.5020
170,603	25.7	1.488	5.867X10 ⁻⁵	25.7	28.97	21	0	79	0	.5020
183,728	14.9	.889	3.511X10 ⁻⁵	14.9	28.97	21	0	79	0	.5020
196,848	-4.7	5.30X10 ⁻¹	2.180X10 ⁻⁵	-4.7	28.97	21	0	79	0	.5020
209,971	-29.6	3.07X10 ⁻¹	1.538X10 ⁻⁵	-29.6	28.97	21	0	79	0	.5020
223,094	-58.0	1.72X10 ⁻¹	8.024X10 ⁻⁶	-58.0	28.97	21	0	79	0	.5020
236,217	-75.2	9.55X10 ⁻²	4.543X10 ⁻⁶	-75.2	28.97	21	0	79	0	.5020
249,340	-85.5	4.95X10 ⁻²	2.480X10 ⁻⁶	-85.5	28.97	21	0	79	0	.5020
262,464	-90.7	2.58X10 ⁻²	1.518X10 ⁻⁶	-90.7	28.97	21	0	79	0	.5020
276,588	-83.3	1.15X10 ⁻²	8.781X10 ⁻⁷	-83.2	28.23	17.9	5.1	77	0	.5020
289,712	-89.1	5.51X10 ⁻³	2.840X10 ⁻⁷	-88.6	27.52	15.0	10.0	75	0	.5020
311,876	-50.2	2.51X10 ⁻³	1.151X10 ⁻⁷	-80.1	28.86	12.2	14.8	73.2	0	.5020
328,080	-27.7	1.24X10 ⁻³	6.375X10 ⁻⁸	-88.6	26.22	9.5	19.0	71.5	0	.5020
344,484	-7.4	6.35X10 ⁻⁴	2.811X10 ⁻⁸	-54.2	25.81	7.0	23.2	69.8	0	.5020
360,888	28.3	3.58X10 ⁻⁴	1.292X10 ⁻⁸	-33.8	25.03	4.5	27.2	68.3	0	.5020
377,292	80.3	1.88X10 ⁻⁴	8.522X10 ⁻⁹	-8.8	24.48	2.2	31.0	66.8	0	.5020
393,696	134.3	1.11X10 ⁻⁴	3.519X10 ⁻⁹	31.3	23.96	0	34.7	65.3	0	.5020
410,100	188.3	6.92X10 ⁻⁵	1.997X10 ⁻⁹	58.3	23.19	0	33.6	60.1	6.3	.5020
428,504	242.3	04.47X10 ⁻⁵	1.190X10 ⁻⁹	85.5	22.50	0	32.8	55.2	12.2	.5020
442,908	294.5	2.98X10 ⁻⁵	7.388X10 ⁻¹⁰	107.5	21.83	0	31.6	50.5	17.9	.5020
459,312	344.9	2.06X10 ⁻⁵	4.747X10 ⁻¹⁰	129.4	21.21	0	30.7	48.2	23.1	.5020
476,716	395.3	1.43X10 ⁻⁵	3.158X10 ⁻¹⁰	148.3	20.58	0	29.8	42.1	28.1	.5020
492,120	445.7	1.03X10 ⁻⁵	2.125X10 ⁻¹⁰	151.4	20.06	0	29.0	38.2	32.8	.5020
508,524	498.1	7.80X10 ⁻⁶	1.467X10 ⁻¹⁰	185.0	19.49	0	28.3	34.5	37.2	.5020
524,928	548.3	5.57X10 ⁻⁶	1.034X10 ⁻¹⁰	202.7	18.05	0	27.5	31.1	41.4	.5020
557,736	653.9	3.21X10 ⁻⁶	6.412X10 ⁻¹¹	236.3	19.10	0	26.2	24.8	49.2	.5020
590,544	758.7	1.95X10 ⁻⁶	3.002X10 ⁻¹¹	288.4	17.28	0	24.9	18.8	58.3	.5020
623,352	863.1	1.24X10 ⁻⁶	1.781X10 ⁻¹¹	293.8	16.50	0	23.8	15.5	62.7	.5020
658,160	968.8	8.11X10 ⁻⁷	1.065X10 ⁻¹¹	318.1	15.79	0	22.8	9.8	68.8	.5020
688,968	1069.9	5.49X10 ⁻⁷	6.720X10 ⁻¹²	340.2	15.15	0	21.9	4.1	74.0	.5020
721,776	1172.2	3.82X10 ⁻⁷	4.379X10 ⁻¹²	360.2	14.55	0	21.0	0	79.0	.5020

^aAssumed from theoretical calculations above 262,464 ft; no rocket data available in 1952.^bPresented at "odd" altitudes because original model was in oga units.^cPressure above 428,504 ft is extrapolated.

TABLE II. - HULLBERT-JEL: EXTRAPOLATED ATMOSPHERIC MODEL (REF. 3)

[Converted to engineering units.]

Altitude (above sea level), ft (b)	Physical properties			Chemical composition ^a					
	Temp. for varying \bar{M} , °F	Pressure, lb(ℱ)/sq ft	Density, lb(M)/cu ft	Average molecular weight, \bar{M} , lb/lb-mole	Volume percent O ₂	Volume percent O	Volume percent N ₂	Volume percent N	Weight ratio, Oxygen Nitrogen
0	62.5	2091	7.461×10 ⁻²	28.8	21	0	79	0	0.3038
32,808	-45.7	577	2.598×10 ⁻²	28.8	21	0	79	0	.3038
65,618	-81.7	115	5.670×10 ⁻³	28.8	21	0	79	0	.3038
98,424	-56.7	26.4	1.164×10 ⁻³	28.8	21	0	79	0	.3038
131,232	8.3	6.67	2.658×10 ⁻⁴	28.8	21	0	79	0	.3038
164,040	26.3	1.87	7.182×10 ⁻⁵	28.8	21	0	79	0	.3038
198,848	-18.7	5.23×10 ⁻¹	2.208×10 ⁻⁵	28.8	21	0	79	0	.3038
229,656	-81.7	1.21×10 ⁻¹	5.989×10 ⁻⁶	28.8	21	0	79	0	.3038
262,464	-128.7	2.19×10 ⁻²	1.224×10 ⁻⁶	28.8	21	0	79	0	.3038
295,272	-130.3	3.48×10 ⁻³	1.970×10 ⁻⁷	28.8	21	0	79	0	.3038
328,080	-99.7	6.34×10 ⁻⁴	3.223×10 ⁻⁸	28.8	20	1	79	0	.2865
360,888	-45.7	1.33×10 ⁻⁴	5.598×10 ⁻⁹	27.0	11	14	75	0	.2743
393,696	44.3	4.12×10 ⁻⁵	1.337×10 ⁻⁹	25.3	7	24	69	0	.3147
426,504	301.7	9.25×10 ⁻⁵	5.484×10 ⁻¹⁰	25.2	6	25	69	0	.3064
459,312	609.5	9.93×10 ⁻⁶	1.503×10 ⁻¹⁰	25.0	5	26	69	0	.2981
492,120	886.9	6.38×10 ⁻⁶	7.616×10 ⁻¹¹	24.5	5	28	65	4	.3070
524,928	1063.1	4.64×10 ⁻⁶	4.666×10 ⁻¹¹	23.7	4.4	28	60	7.6	.3296
557,736	1209.5	3.47×10 ⁻⁶	3.098×10 ⁻¹¹	23.0	3.9	32	53	9.1	.3819
590,544	1302.5	2.63×10 ⁻⁶	2.149×10 ⁻¹¹	22.3	3.3	35	50	11.7	.4258
623,352	1370.9	2.05×10 ⁻⁶	1.574×10 ⁻¹¹	21.7	2.8	39	46	12.2	.4892
656,160	1417.7	1.62×10 ⁻⁶	1.181×10 ⁻¹¹	21.1	2.5	44	41	12.5	.5626
721,776	1473.5	1.06×10 ⁻⁶	7.046×10 ⁻¹²	20.0	1.8	51	34	13.2	.7885
787,392	1498.7	7.21×10 ⁻⁷	4.576×10 ⁻¹²	19.2	1.3	56	27	15.7	.9609
853,008	1511.3	5.08×10 ⁻⁷	3.017×10 ⁻¹²	18.2	.9	60	20	19.1	1.195
918,624	1516.7	3.49×10 ⁻⁷	1.995×10 ⁻¹²	17.5	.7	65	15	19.3	1.539
984,240	1520.3	2.44×10 ⁻⁷	1.36×10 ⁻¹²	16.8	.5	67	10	22.5	1.828
1,148,280	1520.3	1.11×10 ⁻⁷	5.91×10 ⁻¹³	16.3	.2	68	7	24.8	2.014
1,312,320	1520.3	4.78×10 ⁻⁸	2.53×10 ⁻¹³	-----	-----	-----	-----	-----	-----
1,476,360	1520.3	1.87×10 ⁻⁸	9.96×10 ⁻¹⁴	-----	-----	-----	-----	-----	-----
1,640,400	1520.3	9.83×10 ⁻⁹	5.24×10 ⁻¹⁴	-----	-----	-----	-----	-----	-----

^aChemical composition above 426,504 ft is based on theoretical calculations.^bPresented at "odd" altitudes because original model was in cgs units.^cPressure above 426,504 ft is extrapolated.^dDensity above 721,776 ft is extrapolated.

TABLE III. - THE ARDC MODEL ATMOSPHERE, 1958

Altitude (above sea level), ft (b)	Physical properties			Chemical composition ^a					
	Temp. for varying μ , OF	Pressure, lb(F)/sq ft	Density, lb(M)/cu ft	Average molecular weight, μ , lb/lb-mole	Volume percent O ₂	Volume percent O	Volume percent N ₂	Volume percent N	Weight ratio, Oxygen Nitrogen
246,075	-99.2	5.95x10 ⁻²	3.095x10 ⁻⁶	28.97	21	0	79	0	0.3020
262,464	-105.3	2.55x10 ⁻²	1.352x10 ⁻⁶	28.97	21	0	79	0	.3020
295,272	-105.3	4.71x10 ⁻³	2.494x10 ⁻⁷	28.97	21	0	79	0	.3020
328,080	-87.1	9.66x10 ⁻⁴	4.446x10 ⁻⁸	28.0	8.5	20.5	71.0	0	.3000
360,888	-49.0	2.47x10 ⁻⁴	9.920x10 ⁻⁹	25.0	4.1	27.6	68.1	.2	.2982
393,696	-5.8	7.53x10 ⁻⁵	2.670x10 ⁻⁹	24.8	2.9	29.8	67.7	.6	.2974
426,504	53.2	^c 2.62x10 ⁻⁵	8.109x10 ⁻¹⁰	24.5	2.8	29.6	66.5	1.1	.2982
459,312	193.2	1.11x10 ⁻⁵	2.682x10 ⁻¹⁰	24.4	2.3	29.4	68.2	2.1	.2872
492,120	332.3	5.63x10 ⁻⁶	1.11x10 ⁻¹⁰	24.2	1.9	29.2	65.7	3.2	.2785
574,175	676.7	1.58x10 ⁻⁶	2.153x10 ⁻¹¹	23.8	.7	32.4	62.0	4.9	.2979
656,160	822.3	6.13x10 ⁻⁷	6.926x10 ⁻¹²	22.6	.6	35.5	55.4	8.5	.3495
738,225	922.4	2.73x10 ⁻⁷	^d 2.689x10 ⁻¹²	20.7	.5	41.5	48.0	10.0	.4555
820,250	1024.4	1.34x10 ⁻⁷	1.177x10 ⁻¹²	20.1	.4	50.2	36.0	13.4	.6785
902,275	1127.5	7.21x10 ⁻⁸	5.663x10 ⁻¹³	18.9	.3	54.6	30.0	15.1	.8351
984,240	1231.0	4.11x10 ⁻⁸	2.936x10 ⁻¹³	18.5	.3	59.0	23.2	17.5	1.060
1,066,272	1334.7	2.47x10 ⁻⁸	1.622x10 ⁻¹³	17.8	.3	61.8	17.9	20.0	1.271
1,148,280	1438.1	1.55x10 ⁻⁸	9.393x10 ⁻¹⁴	17.5	.2	64.5	13.3	22.0	1.517
1,230,315	1541.3	1.01x10 ⁻⁸	5.713x10 ⁻¹⁴	17.1	.1	66.5	10.7	22.7	1.718
1,312,320	1644.1	6.81x10 ⁻⁹	3.582x10 ⁻¹⁴	16.8	.1	66.5	10.6	22.8	1.722
1,394,355	1746.5	4.71x10 ⁻⁹	2.328x10 ⁻¹⁴	16.6	0	67.7	9.3	23.0	1.849
1,476,360	1848.4	3.33x10 ⁻⁹	1.556x10 ⁻¹⁴	16.4	0	67.6	8.3	24.1	1.887
1,558,400	1949.7	2.42x10 ⁻⁹	1.071x10 ⁻¹⁴	16.2	0	66.7	6.6	26.7	1.899
1,640,400	2050.4	1.78x10 ⁻⁹	7.471x10 ⁻¹⁵	16.1	0	68.2	5.6	26.2	2.071

^aEstimated from graph in ref. 5.^bPresented at "odd" altitudes to match other tables.^cPressure above 426,504 ft is extrapolated.^dDensity above 721,776 ft is extrapolated.

TABLE IV. - VERTICAL DISTRIBUTION OF ATOMIC OXYGEN AND OZONE

(REF. 3)

Altitude, ft	Ozone		Atomic oxygen	
	Concentration of O ₃ , molecule/cc	Volume percent	Concentration of O, molecule/cc	Volume percent
49,212	1.0×10 ¹¹	2.44×10 ⁻⁵	-----	-----
65,616	2.0×10 ¹²	1.05×10 ⁻⁴	-----	-----
98,424	6.7×10 ¹²	1.72×10 ⁻³	1.7×10 ⁹	4.36×10 ⁻⁷
131,232	4.8×10 ¹¹	5.39×10 ⁻⁴	2.0×10 ¹⁰	2.25×10 ⁻⁵
164,040	4.3×10 ¹⁰	1.79×10 ⁻⁴	4.4×10 ¹⁰	1.83×10 ⁻⁴
196,848	7.0×10 ⁹	9.46×10 ⁻⁵	1.0×10 ¹¹	1.35×10 ⁻³
229,656	1.2×10 ⁹	6.00×10 ⁻⁵	1.9×10 ¹¹	9.50×10 ⁻³
262,464	7.6×10 ⁷	1.85×10 ⁻⁵	2.7×10 ¹¹	6.59×10 ⁻²
295,272	5.0×10 ⁶	7.58×10 ⁻⁶	3.3×10 ¹¹	0.50

TABLE V. - UPPER AND LOWER LIMITS OF ATOMIC OXYGEN RECOMBINATION

IN NOZZLE OF RAMJET ORBITING AT 328,080 FEET IN ATMOSPHERE

OF TABLE I

[Nozzle length, 100 ft; frozen-compression diffuser.]

Recombination- rate coefficient, k _r , ($\frac{\text{g-mole}}{\text{liter}}$) ⁻² sec ⁻¹	Near-equilibrium limit		Near-frozen limit	
	% O, $\frac{\text{g-mole O}}{\text{liter}}$	Minimum mass percent recombined	% O, $\frac{\text{g-mole O}}{\text{liter}}$	Maximum mass percent recombined
10 ¹¹	5.3×10 ⁻²	0	3.2×10 ⁻⁶	8
10 ¹²	5.3×10 ⁻³	0	1.0×10 ⁻⁶	32
10 ¹³	5.3×10 ⁻⁴	0	2.7×10 ⁻⁷	57
10 ¹⁴	5.3×10 ⁻⁵	0	6.6×10 ⁻⁸	78
10 ¹⁵	3.7×10 ⁻⁶	4	1.4×10 ⁻⁸	91
10 ¹⁶	1.2×10 ⁻⁶	29	2.7×10 ⁻⁹	97

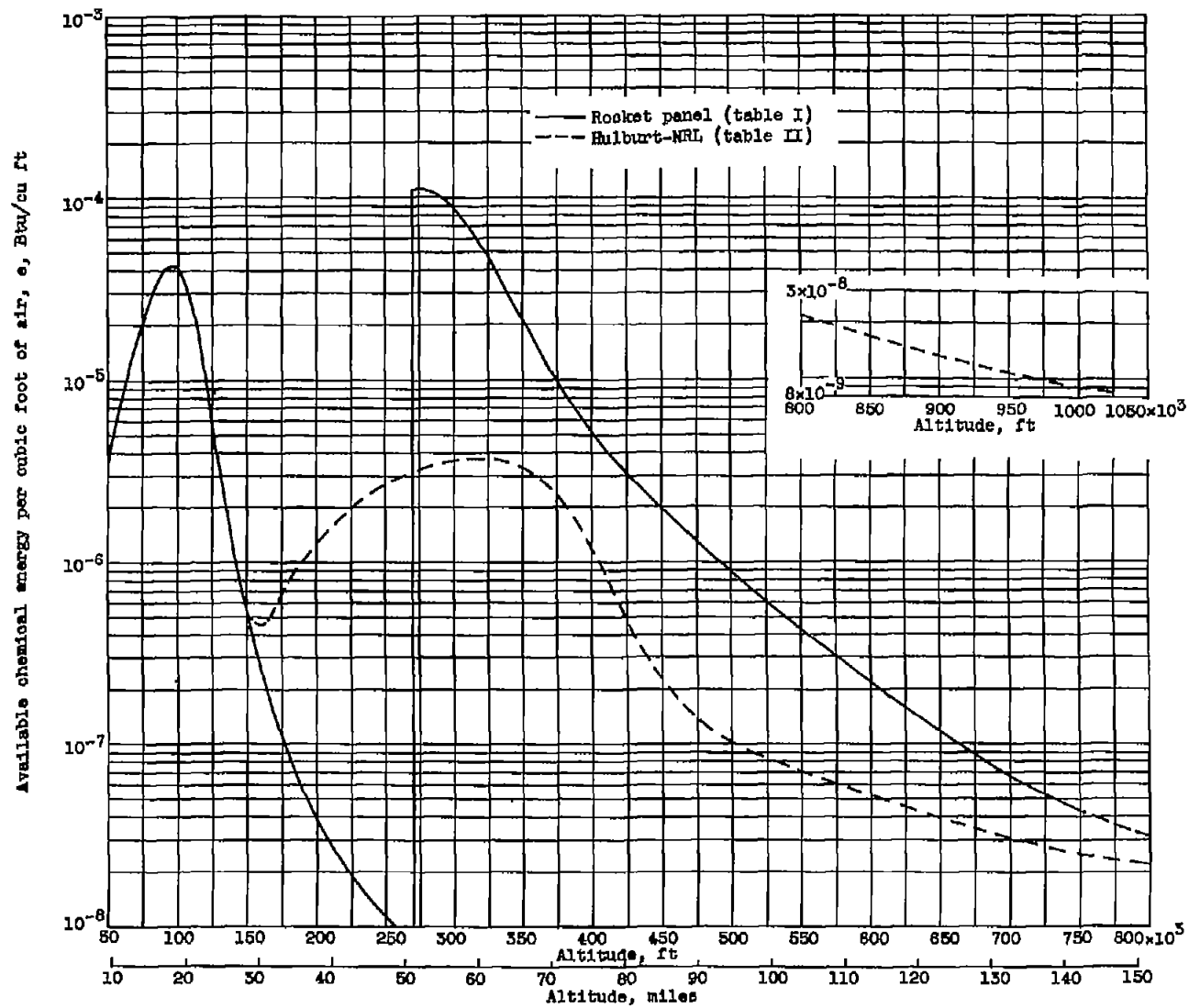


Figure 1. - Available chemical-energy density in the upper atmosphere.

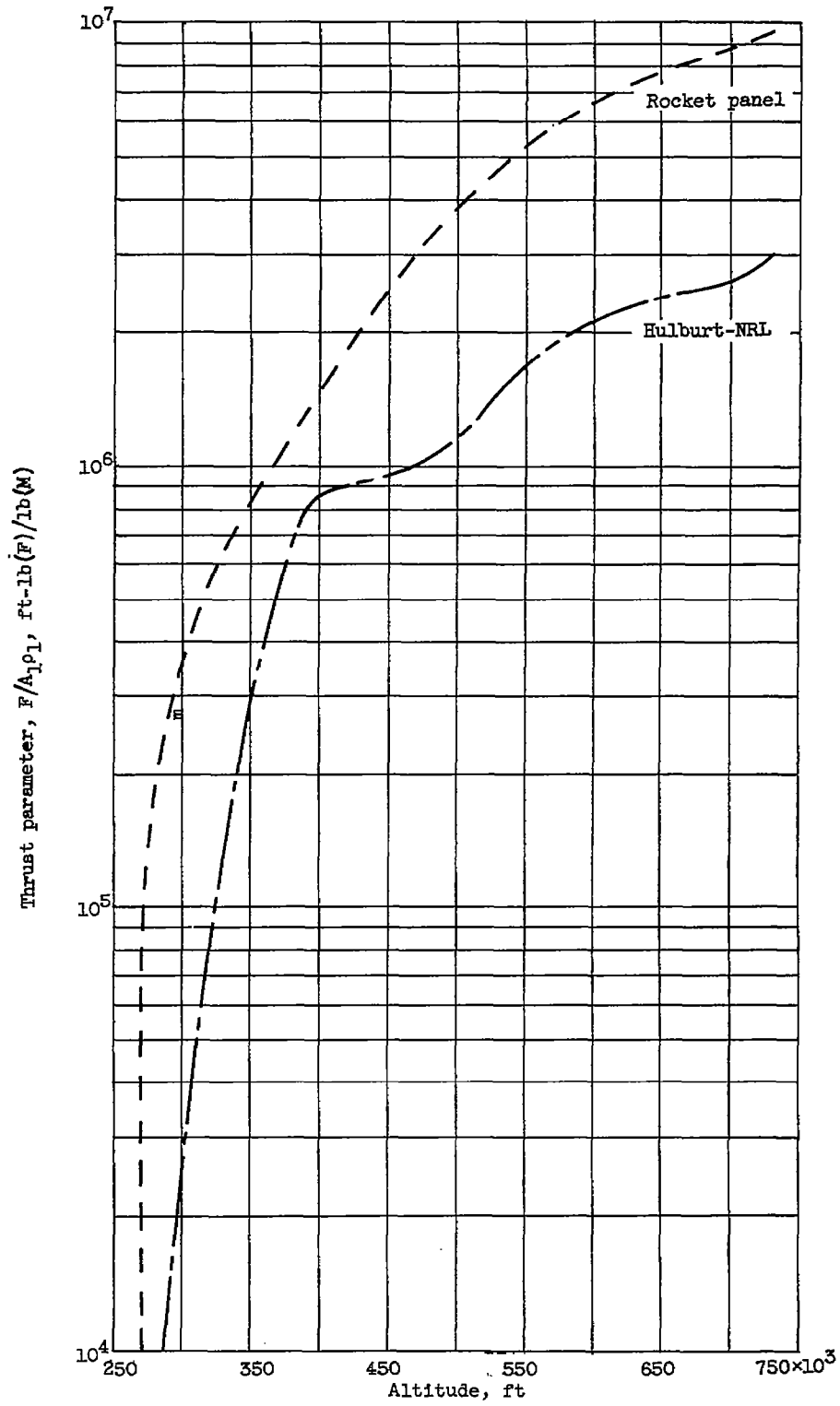
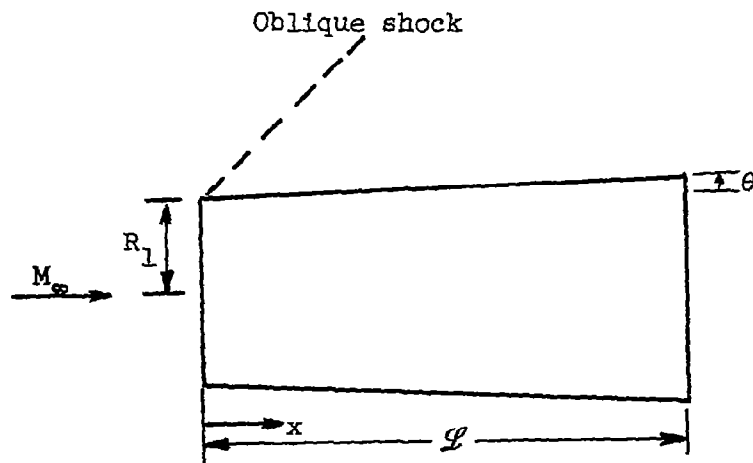
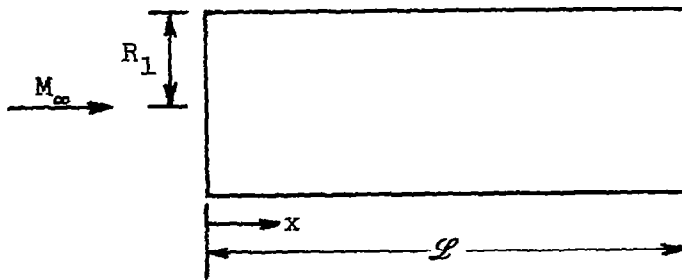


Figure 2. - Variation of atmospheric energy available for propulsion with altitude.

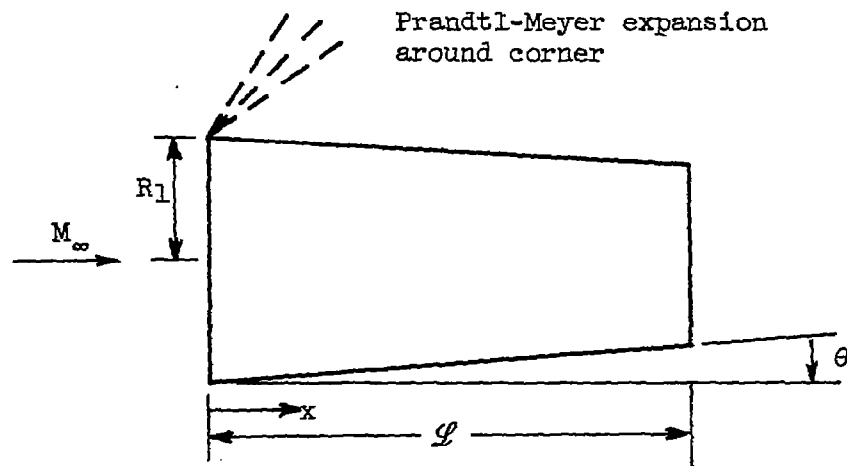
4780



(a) Configuration I: Truncated cone.

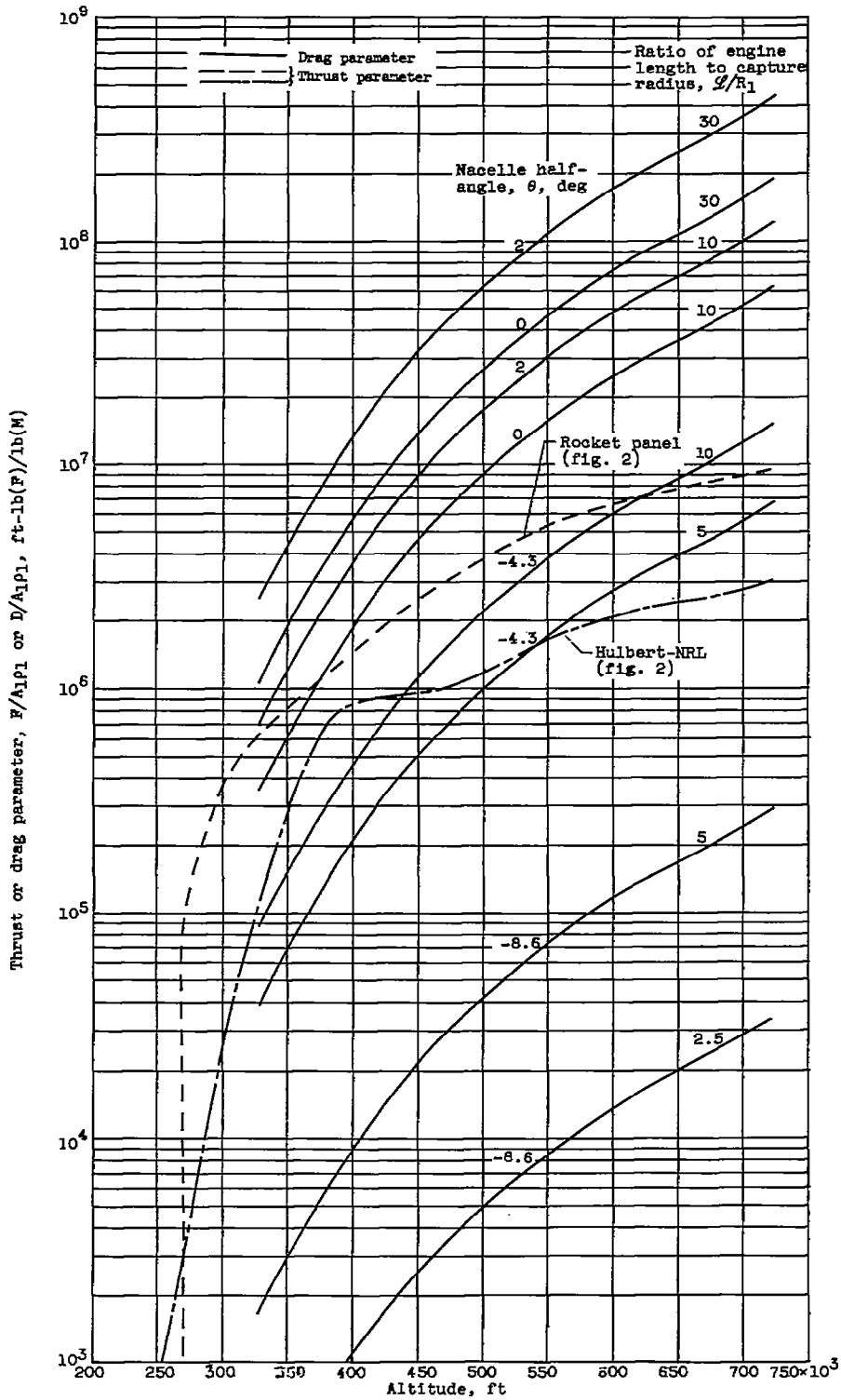


(b) Configuration II: Circular cylinder.



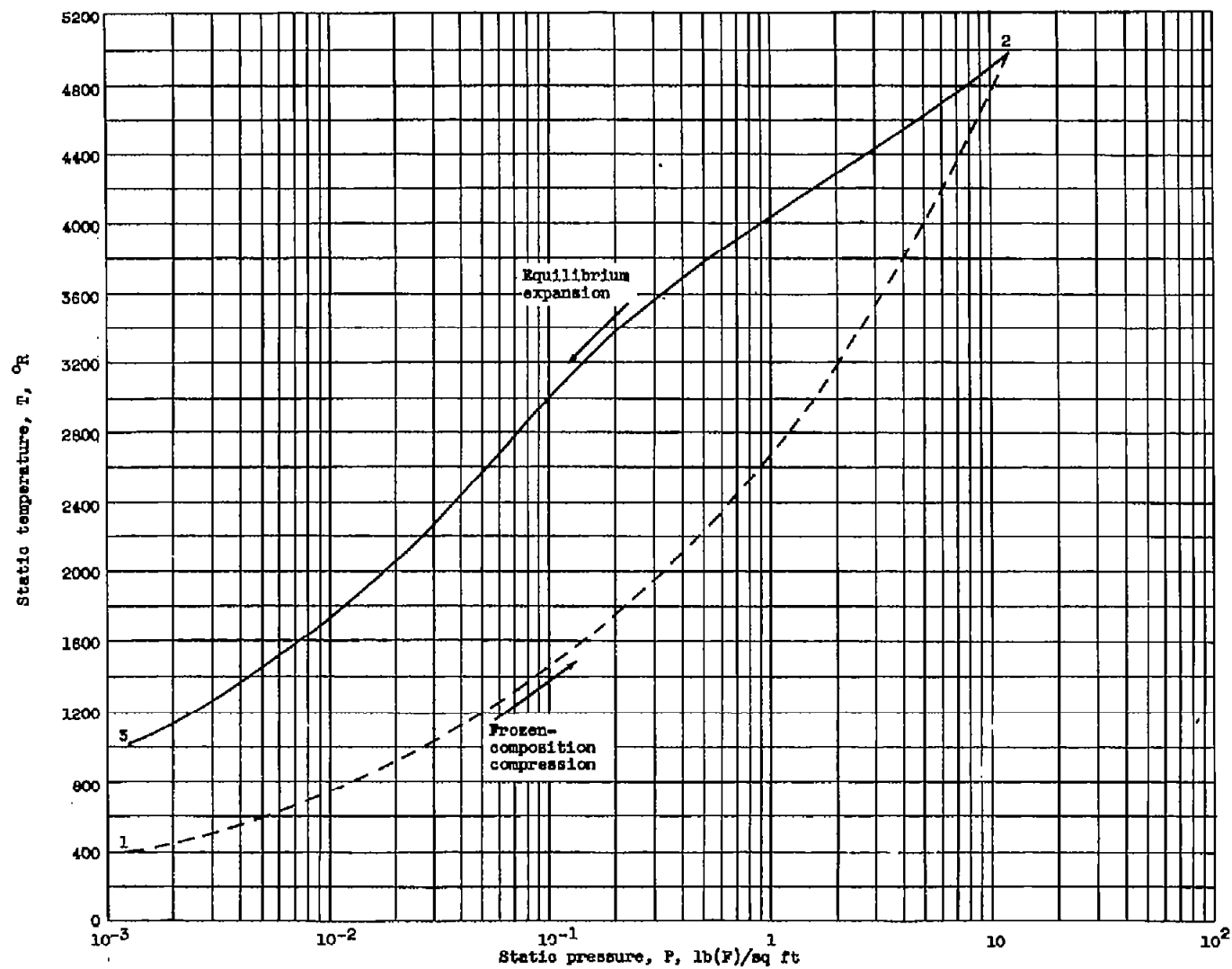
(c) Configuration III: Reversed truncated cone.

Figure 3. - Nacelle geometries for recombination ramjet.



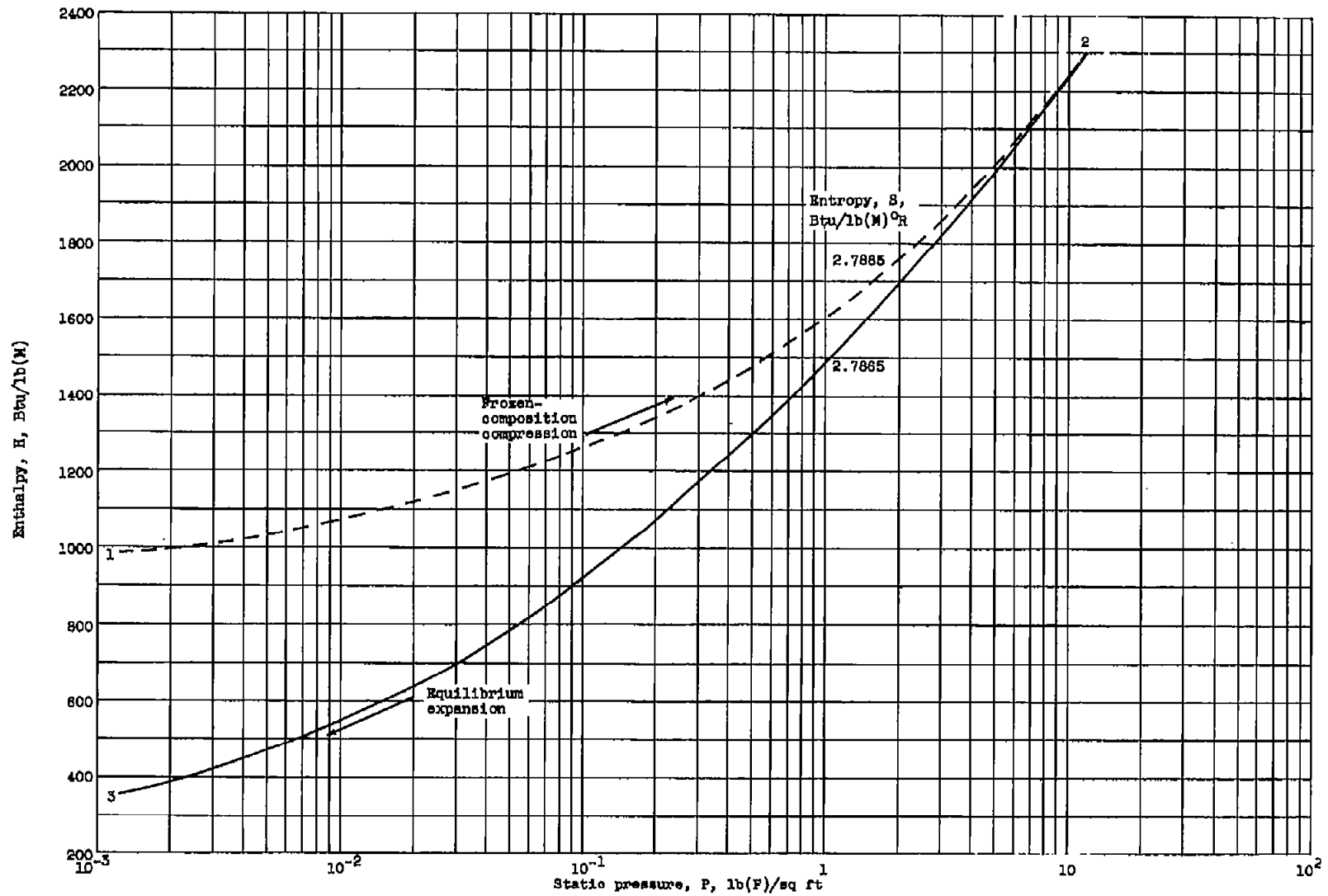
(b) Engine length, 1000 feet.

Figure 4. - Concluded. Comparison of energy available with energy required for sustaining ionosphere orbits. Wall temperature, 1000° R.



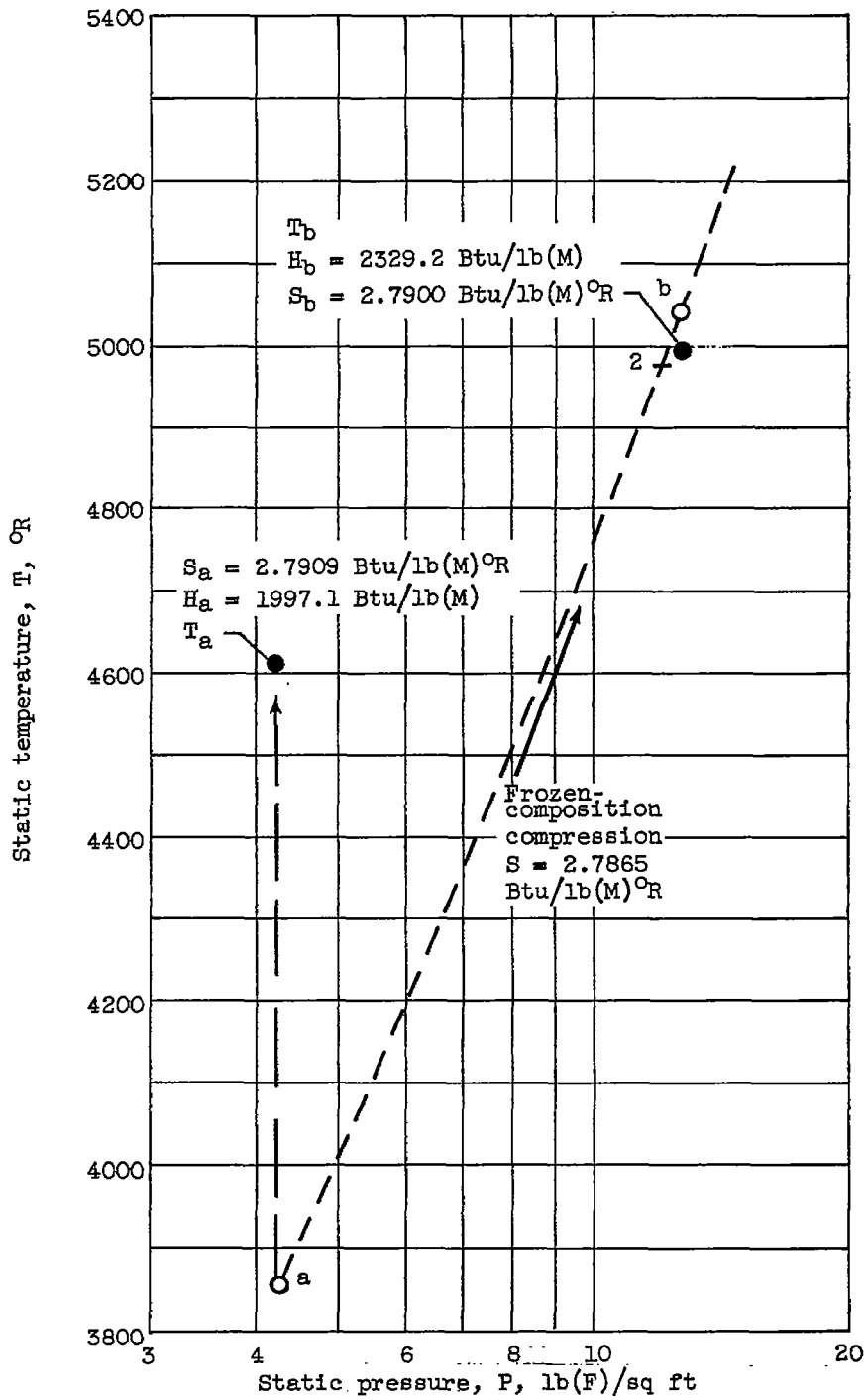
(a) Variation of temperature and pressure.

Figure 5. - Thermodynamic cycle for ionosphere ramjet orbiting at 328,080 feet.



(b) Variation of enthalpy and pressure.

Figure 5. - Continued. Thermodynamic cycle for ionosphere ramjet orbiting at 328,080 feet.



(c) Temperature-pressure detail for determining compression-termination station 2.

Figure 5. - Concluded. Thermodynamic cycle for ionosphere ramjet orbiting at 328,080 feet.

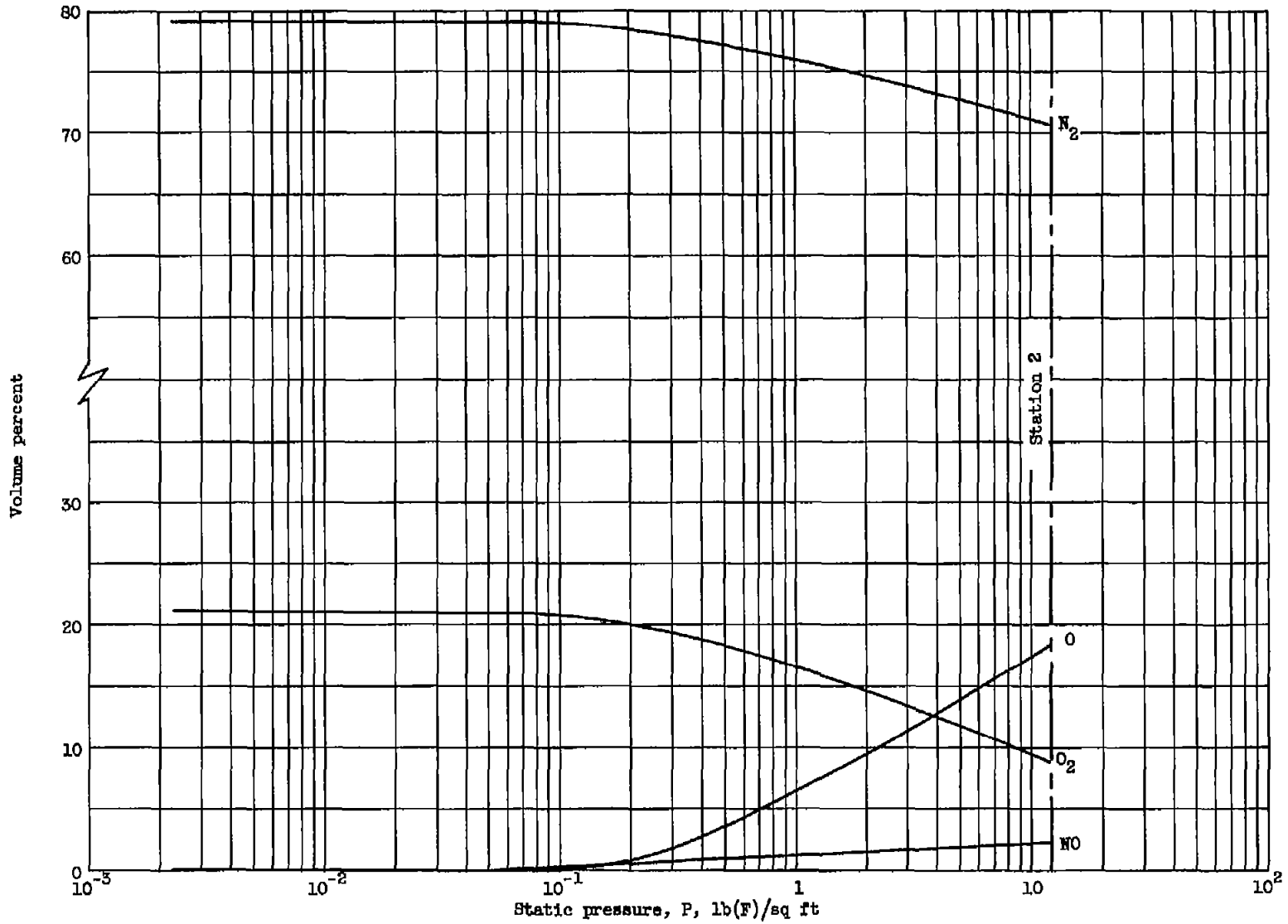


Figure 6. - Chemical composition in equilibrium expansion of ramjet cycle of figure 5.

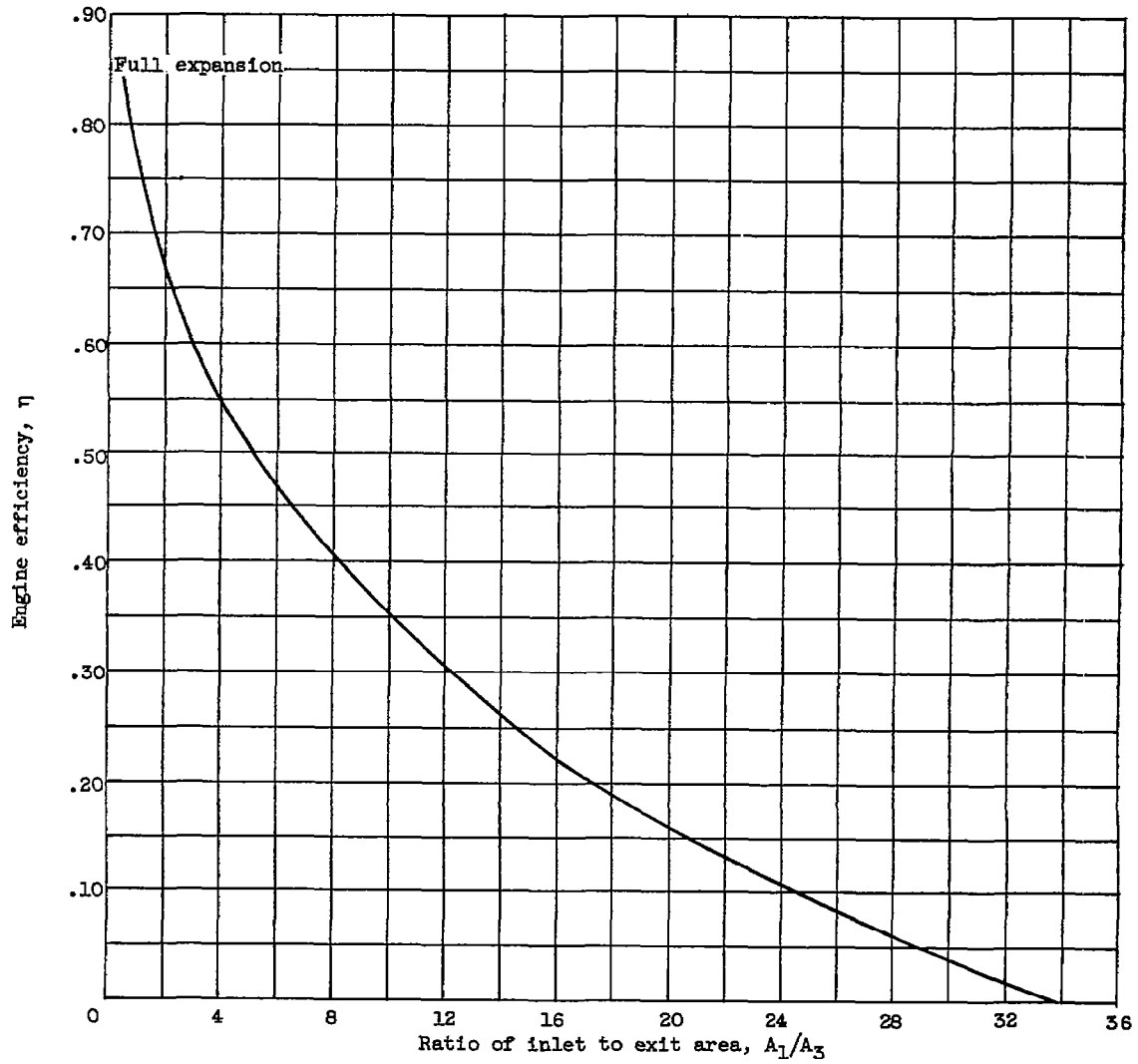


Figure 7. - Effect of ratio of inlet to exit area on ideal over-all engine efficiency for ramjet cycle of figure 5.

4780

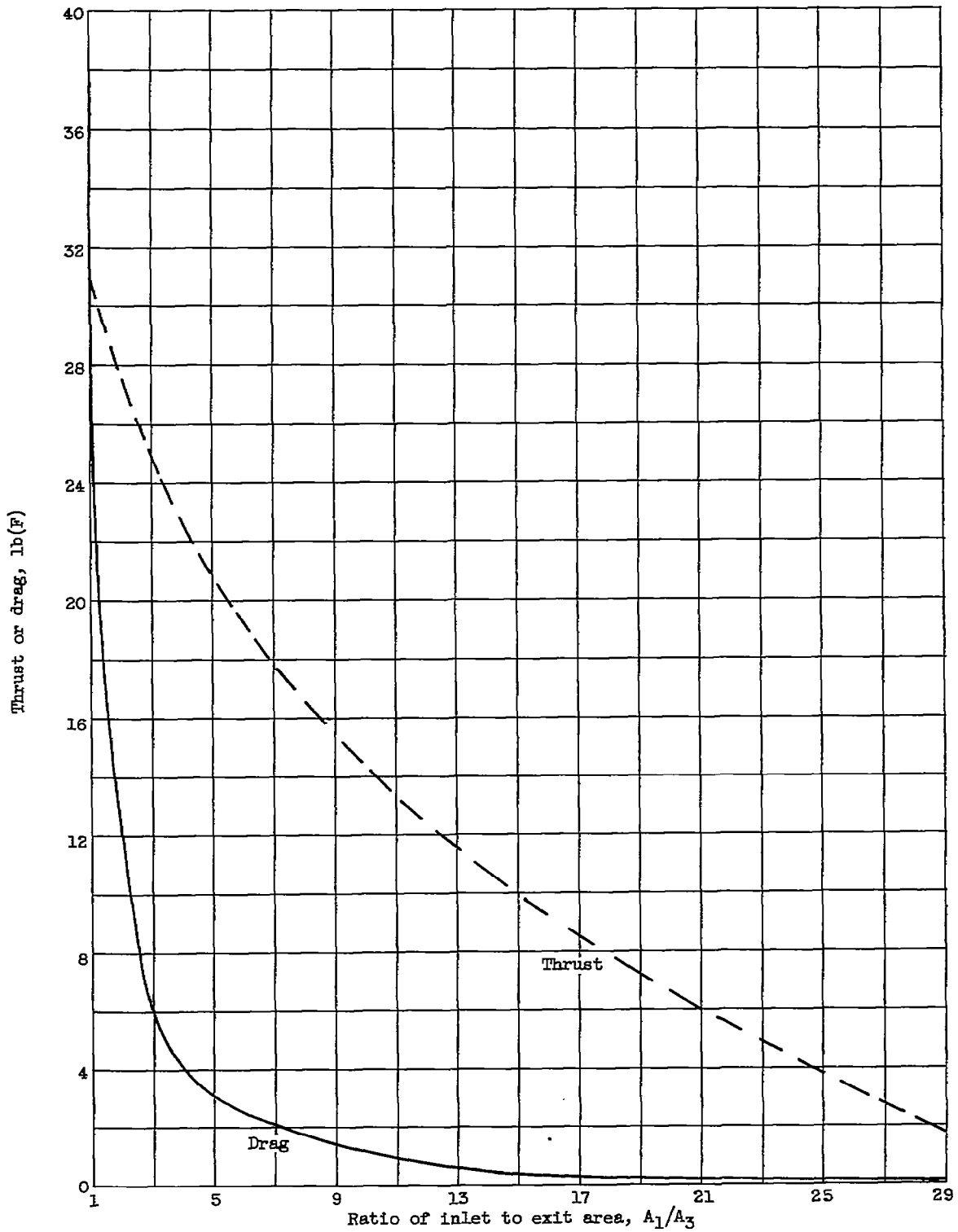


Figure 8. - Effect of ratio of inlet to exit area on thrust and drag for ramjet cycle of figure 5. Engine length, 100 feet; inlet radius, 20 feet.

4780

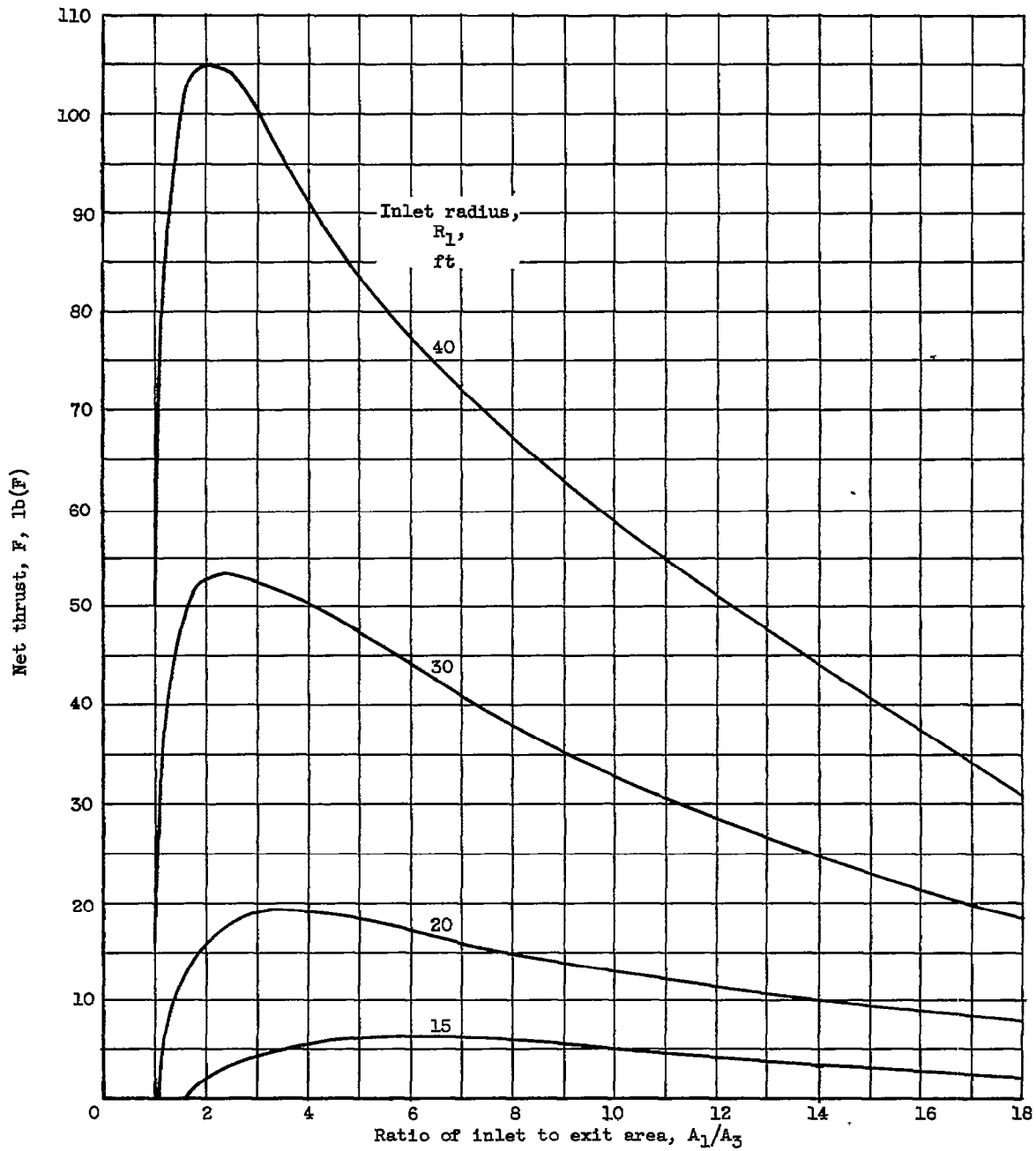


Figure 9. - Variation of net thrust for ramjet cycle of figure 5 with ratio of inlet to exit area for various inlet radii. Engine length, 100 feet.

4780

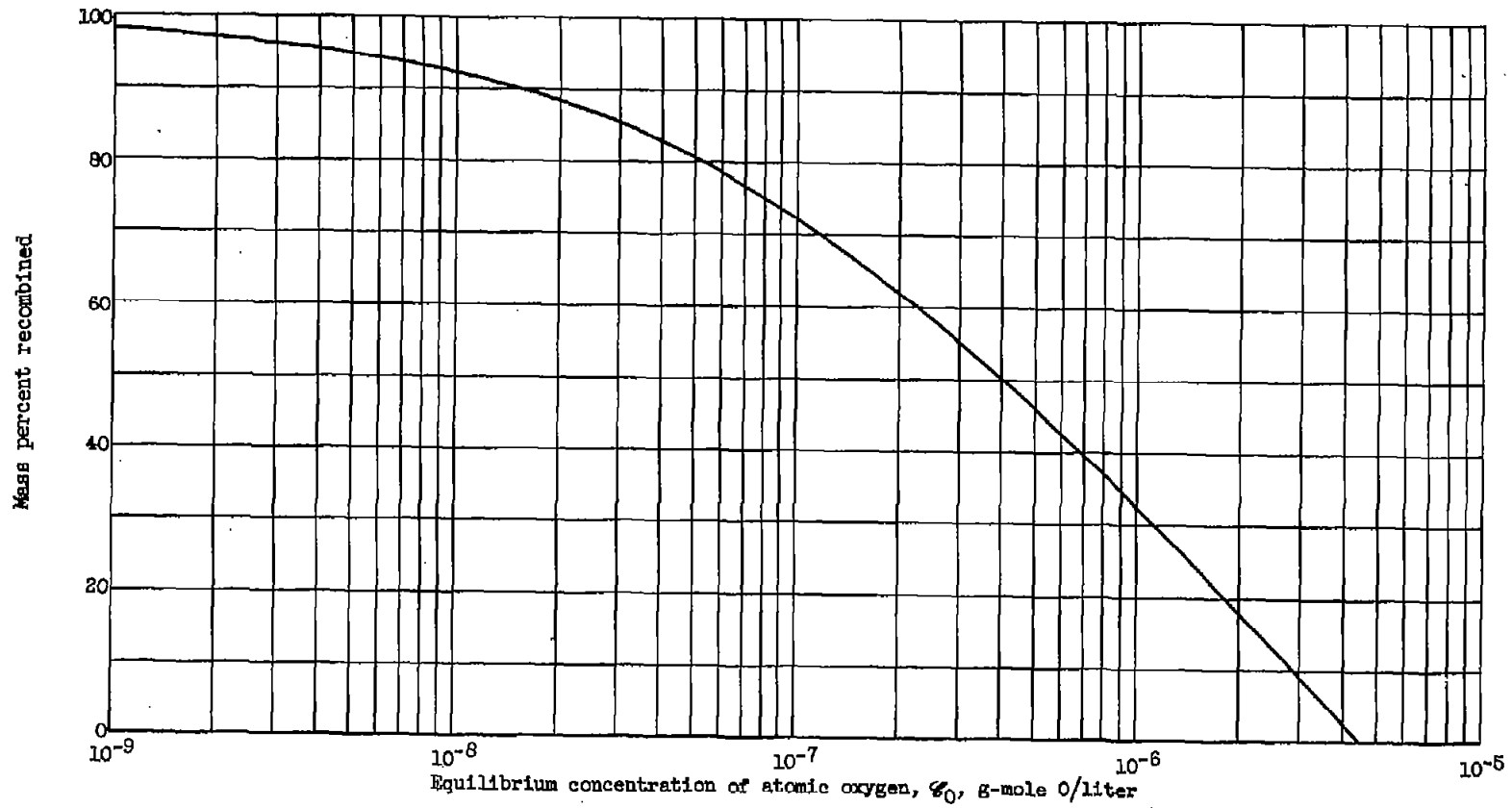


Figure 10. - Relation between mass percentage recombined and atomic oxygen concentration in exhaust nozzle for ramjet cycle of figure 5.

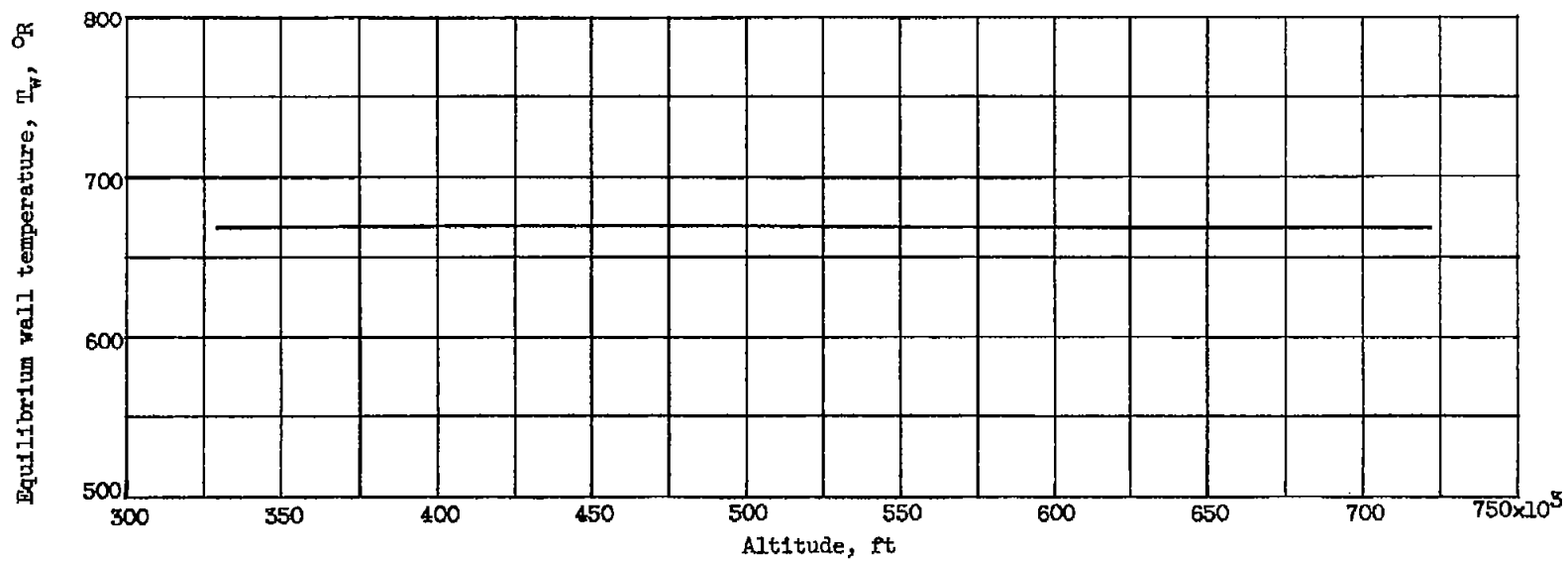


Figure 11. - Variation of external equilibrium wall temperature with altitude. Engine length, 100 feet; nacelle half-angle, -8.6° ; sunny side.

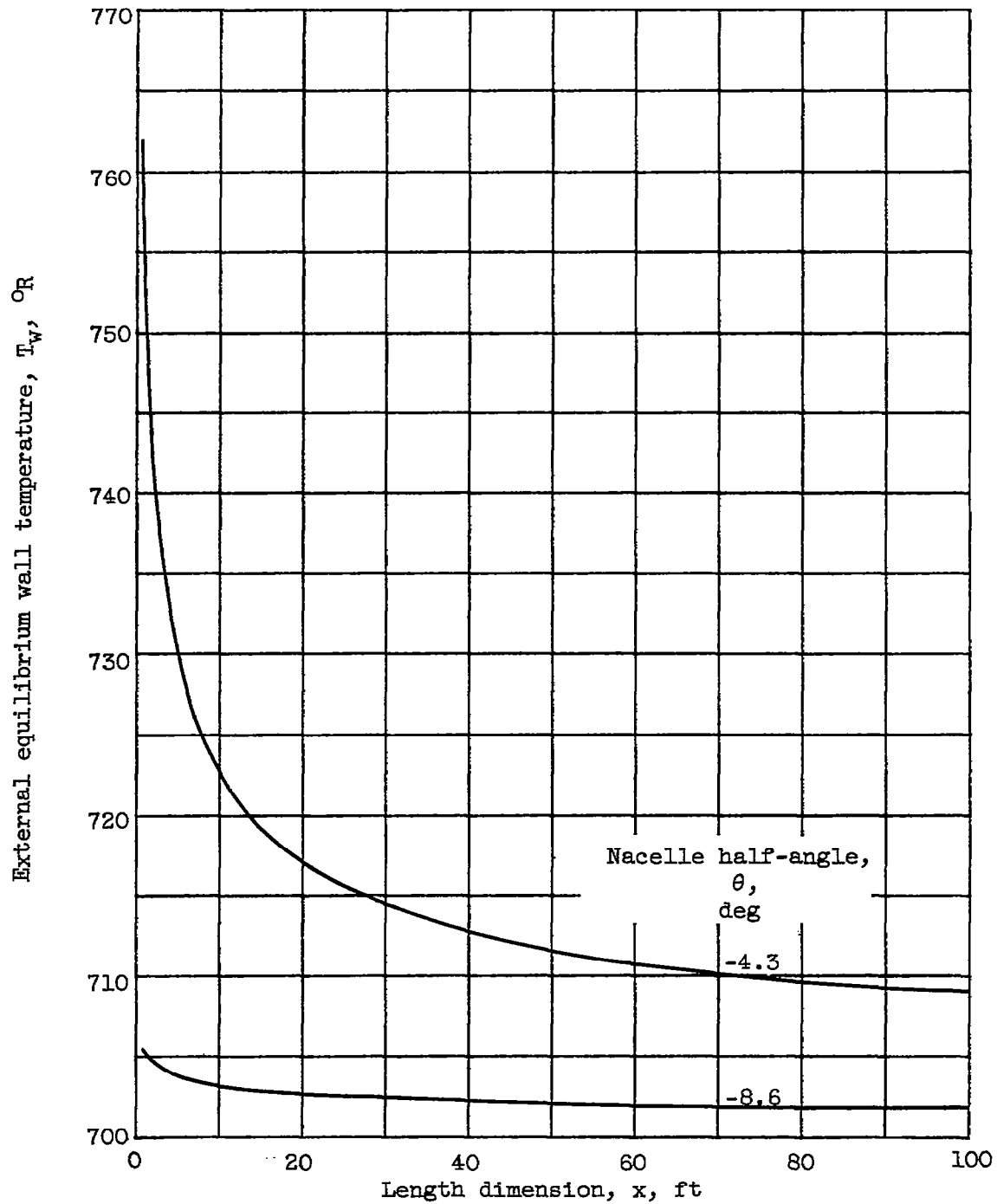


Figure 12. - Variation of external equilibrium wall temperature with nacelle length. Altitude, 328,080 feet; sunny side.